# Geometrical characteristics of magnetospheric energetic ion time series: evidence for low dimensional chaos

**G. P. Pavlos, M. A. Athanasiu, A. G. Rigas, D. V. Sarafopoulos, and E. T. Sarris**

Department of Electrical and Computer Engineering, Demokritos Univercity of Thrace, 67100 Xanthi, Greece

**Abstract.** In the first part of the paper we study the geometrical characteristics of the magnetospheric ions' time series in the reconstructed phase space by using the SVD extended chaotic analysis, and we test the strong null hypothesis supposing that the ions' time series is caused by a linear stochastic process perturbed by a static nonlinear distortion. The SVD reconstructed spectrum of the ions' signal reveals a strong component of high dimensional, external coloured noise, as well as an internal low dimensional nonlinear deterministic component. Also, the stochastic Lorenz system produced by coloured noise perturbation of the deterministic Lorenz system was used as an archetype model in comparison with the dynamics of the magnetrospheric ions.

**Key words.** Magnetospheric physics (energetic particles) – Radio science (nonlinear phenomena)

## 1 Introduction

Many theoretical and experimental studies support the hypothesis that the magnetosphere can be described as a low dimensional chaotic system. Theoretically, it was introduced by Pavlos (1988, 1994), Baker et al. (1990), Klimas et al. (1991, 1992) and Vörös (1991). Experimentally, it was introduced by using the chaotic analysis of magnetospheric time series as has been discussed in Vassiliadis et al. (1990, 1992), Shan et al. (1991), Roberts et al. (1991), Prichard and Price (1992), Pavlos et al. (1992a, 1992b, 1994).

Parallel to these studies a fruitful criticism has been developed about the supposition of magnetospheric chaos, especially in relation to its experimental evidence (Prichard and Price, 1992, 1993; Price and Prichard, 1993; Price et al., 1994; Prichard, 1995), based on the strong null hypotheses for stochasticity of Theiler (Theiler et al., 1992a, b). The above criticism includes the following assertions:

(a) The correlation dimension of the $AE$ index time series cannot be distinguished from that of a stochastic signal with the same power spectrum and amplitude distribution as the original data.

(b) There is no evidence for the existence of low dimensionality according to their estimate of correlation dimension obtained by using Takens' method.

(c) There is some evidence for nonlinearity in the $AE$ index time series. It is not clear whether the nonlinearity of the $AE$ index is the result of the intrinsic dynamics of the magnetosphere or the result of the nonlinearity in the solar wind.

(d) Because the magnetosphere is largely controlled by the solar wind, this alone should provide evidence against the existence of a strange attractor in the $AE$ index, as the magnetosphere is a randomly driven, non-autonomous system.

(e) There is no evidence for low dimensionality of the $AE$ index and no evidence that the $AE$ index can be described by a low dimensional strange attractor.

In a recent series of papers, an extended chaotic analysis has been developed by Pavlos et al. (1999a, b, c), Athanasiu and Pavlos (2001), in which convincing answers to the above criticism against the existence of internal low dimensional and chaotic magnetospheric dynamics have been given. According to these papers the magnetospheric chaos hypothesis is strongly supported by studying the geometrical and dynamical characteristics of the magnetospheric time series and their corresponding nonlinear surrogate data. In these studies a more effective method for constructing surrogate data was used which was developed by Schreiber and Schmitz (1996) and Schreiber (1998). Also in the last study by Pavlos et al. (1999c), the results of the chaotic analysis of the magnetospheric time series are compared with corresponding results obtained by analysing different types of stochastic and deterministic input-output systems. In the same study the
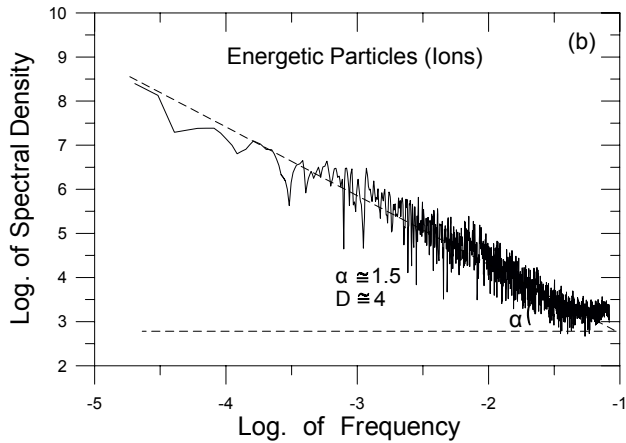
**Fig. 1.** Power spectrum of the full magnetosphere energetic ions time series.

spectrum of the SVD reconstructed components of an experimental time series was used as a tool for discriminating between directly external driven and storage-release magnetospheric processes. Athanasiu and Pavlos (2001) extended this concept of the SVD spectrum analysis to the magnetospheric $AE$ index time series and concluded the existence of an external, strong, high dimensional, coloured component in the magnetospheric $AE$ index, which can be discriminated by including a low dimensional magnetospheric component. Similar results supporting the low dimensional magnetospheric chaos were found by Goode et al. (2001) using $AL$ index data. For a review of studies concerning magnetospheric chaos and nonlinear dynamics applied to the Earth's magnetosphere, refer to Klimas et al. (1996).

In this work the chaotic analysis algorithm is applied for the study of a new magnetospheric time series corresponding to energetic ions. Some evidence for the low dimensional chaotic character of this time series was given by Pavlos et al. (1999c). Moreover, we extend the study of energetic ions time series by examining its geometrical and dynamical characteristics. In Sect. 2 we present some theoretical concepts and results concerning the background of chaotic analysis, including the embedding theory, and the method of SVD analysis. In Sect. 3 we present the results of the chaotic analysis for the energetic ions' time series. Finally, in Sect. 4 we summarise and discuss the conclusions of this paper.

## 2  Theoretical framework

The main purpose of time series analysis is to extract significant information for the underlying dynamics of the observed signal, as well as to develop effective methods for modelling and prediction. Classical time series analysis confronts these problems by using linear or nonlinear input-output methods (Priestley, 1988). On the other hand, the modern analysis of a time series, known as chaotic analysis includes: (a) estimation of the geometrical and dynamical characteristics of

the trajectory of the system in its phase space (Pavlos et al., 1999a, b; Abarbanel et al., 1993; Grassberger and Procaccia, 1983; Tsonis, 1992); (b) testing techniques for the discrimination of low dimensional, nonlinear determinism and linear stochastic processes (Provenzale et al., 1992; Theiler, 1991; Theiler et al., 1992a, b, 1993); (c) forecasting algorithms (Casdagli et al., 1991; Farmer and Sidorowich, 1987; Weigend and Gershenfeld, 1994). The above methods constitute the kernel of the chaotic analysis algorithm. This algorithm has been enriched recently by new results concerning the application of chaotic analysis in known stochastic systems and input-output systems (Argyris et al., 1998a, b; Pavlos et al., 1999a, b, c), as well as by using the SVD analysis for calculating the spectrum of SVD reconstructed components of an experimental time series (Elsner and Tsonis, 1996; Pavlos et al., 1999c; Athanasiu and Pavlos, 2001).

In the following we summarize the main points of the algorithm concerning the chaotic analysis of the experimental signals, which will be used in Sect. 3 for the analysis of the energetic particle signal.

### 2.1  Classical analysis of time series

The classical theory of time series includes the analysis either in the time or in the frequency domains (Tong, 1990; Priestley 1988). Both domains are related by the Wiener-Khintchine theorem according to which if the autocorrelation function of the signal, $C(t)$, sufficiently decays rapidly in time, then the power spectrum is equal to the Fourier transform of the autocorrelation function and is given by

$$P(\omega) = \int_{-\infty}^{\infty} C(\tau)e^{-i\omega\tau}d\tau. \tag{1}$$

In many cases the power spectra of experimental time series approximately follow a power law of the form $P(\omega) \sim \omega^{-\alpha}$. In Fig. 1 the power spectrum of the energetic ions' time series is presented where it can be seen that the exponent $a$ takes values in the range (1, 3). In general, with a stochastic process $x(t)$, with spectrum density proportional to $\omega^{-\alpha}$, it is possible to correspond to a self-affine fractal Brownian motion (fBm), with $H = (\alpha - 1)/2$ and fractal dimension $D = 1/H$ (Osborne and Provenzale, 1989). Because of this, as we show in Sect. 2.7, the Grassberger and Procaccia algorithm cannot distinguish between the deterministic chaotic dynamics and a stochastic fractal system (coloured noise), where small space scales are related to small time scales. It follows from Eq. (1) that when the power spectrum obeys a power law, then the autocorrelation function decays as the lag time $\tau$ increases. These characteristics can be caused by linear-nonlinear stochastic dynamical systems or by low dimensional chaotic dynamical system. Also, the classical time series analysis cannot discriminate between these two cases, while the chaotic analysis, as discussed in the following, can discriminate with high confidence between linear stochasticity and low dimensional chaos.
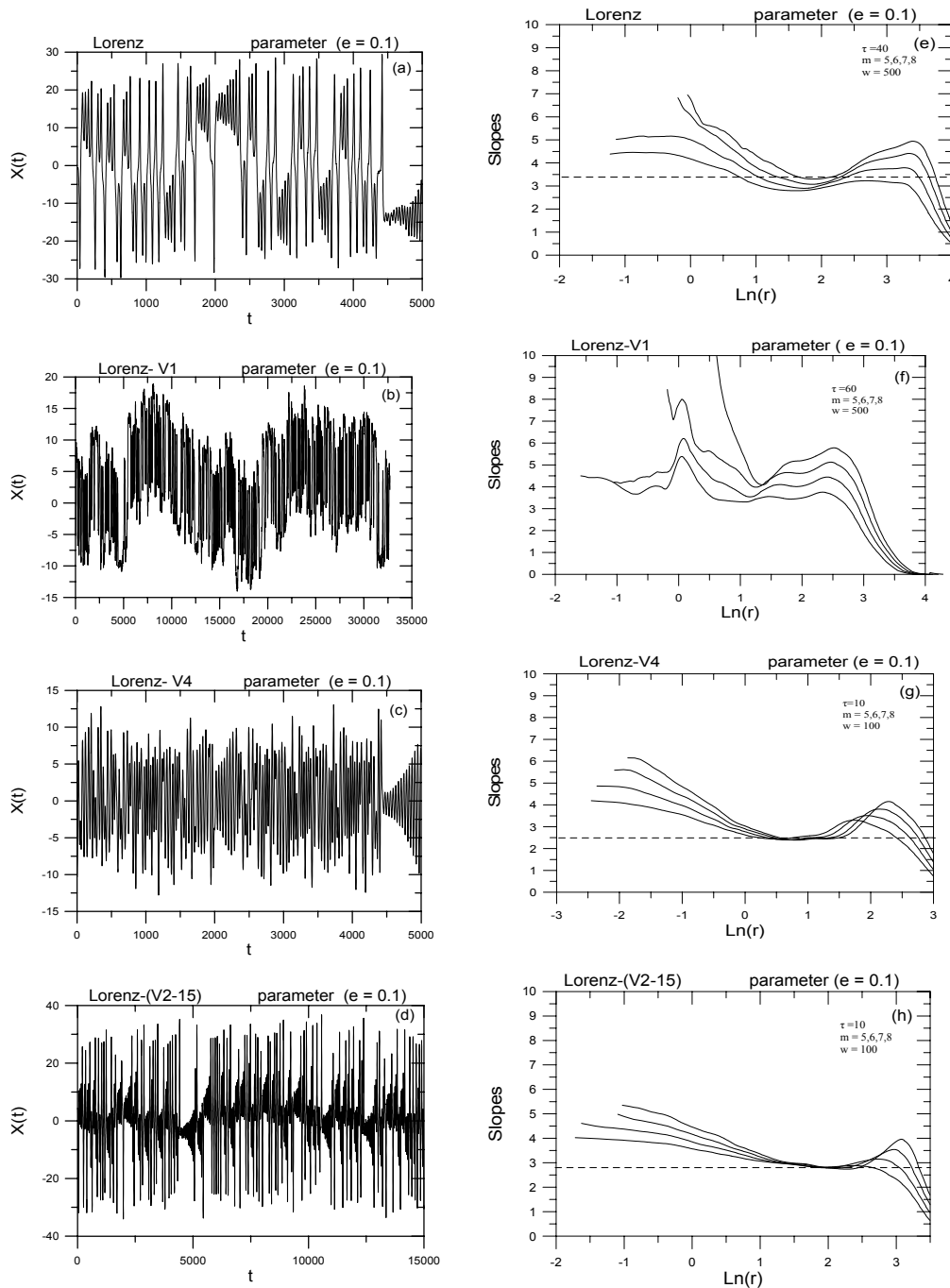
**Fig. 2.** (a)–(d) The stochastic Lorenz signal corresponding to the coloured noise perturbation 37% ($e = 0.1$) and its SVD reconstructed components $V_1$, $V_4$, $V_{2-15}$. The last signal $V_{2-15}$ corresponds to the sum $\sum V_i$, $i = 2 - 15$. (e)–(h) The slopes of the correlation integrals estimated for the signals shown in Fig. 2a–d correspondingly, with embedding $m = 5 - 8$ and $w = 100$.

## 2.2 Embedding theory and phase-space reconstruction

The Earth's magnetosphere is a system of magnetized plasma, which microscopically is an infinite dimensional system, the dynamics of which is mirrored in the ground measured $AE$ index or in the energetic particles' burst observed by spacecraft in situ in the magnetosphere or in the interplanetary space (Pavlos et al., 1999c). Some kind of

"self-organization" may give rise to the system evolution on a low dimensional manifold $\boldsymbol{M}$ of dimension $d$. This means that the magnetosphere can be described macroscopically by a low dimensional dynamical system of $n$ macroscopic degrees of freedom with $n \geq d$. For linear systems, "self-organization" is more an externally driven process described by the external parameters of the system. For nonlinear and dissipative systems, however, it is possible that the system
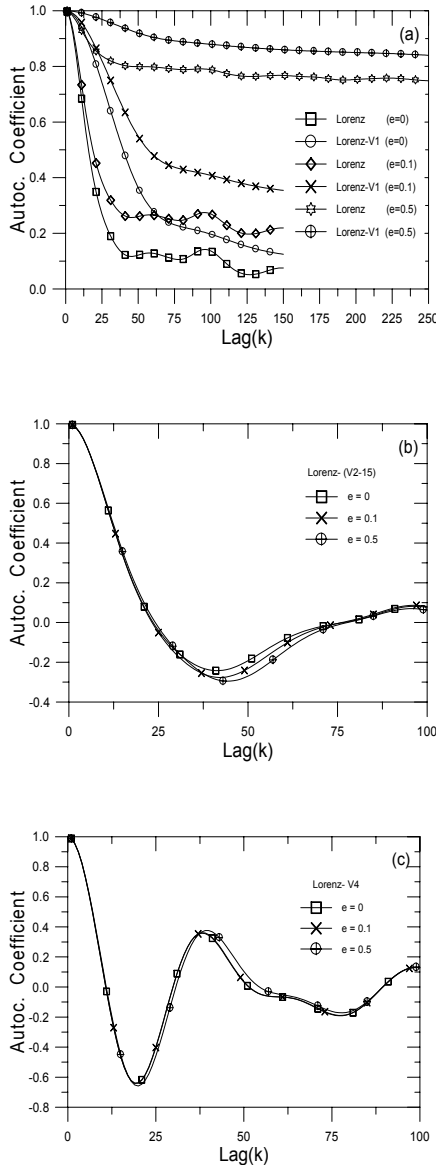
**Fig. 3.** (a) The autocorrelation coefficients of the deterministic $x(t)$ Lorenz signal, of the stochastic $x(t)$ Lorenz signal and its $V_1$ SVD component corresponding to the levels $e = 0.1$ (37%) and $e = 0.5$ (185%) of the external additive coloured noise perturbation. (b) The autocorrelation coefficients of the $V_{2-15}$ SVD component of the stochastic $x(t)$ Lorenz signal corresponding to the two levels $e = 0.1$ (37%) and $e = 0.5$ (185%) of the external additive coloured noise perturbation. (c) The same with Fig. 3b but for the $V_4$ SVD component.

evolves by its internal dynamics in such a way that the corresponding phase space flow contracts on sets of lower dimensions which are called attractors. The embedding theory permits one to study the dynamical characteristics of a physical system by using experimental observations in the form of time series (Takens, 1981; Broomhead and King, 1986). Let $x(t) = f^{(t)}(\boldsymbol{x}(0))$ denote the dynamical flow underlying an experimental time series $x(t_i) = h(\boldsymbol{x}(t_i))$, where $h$

describes the measurement function. When there is a noisy component $w(t_i)$ then the observed time series must be given by $x(t_i) = h(\boldsymbol{x}(t_i), w(t_i))$. On the other hand, Takens (1981) showed that for autonomous and purely deterministic systems, the delay reconstruction map $\Phi$, which maps the states $\boldsymbol{x}$ into m-dimensional delay vectors

$$\Phi(\boldsymbol{x}) = [h(\boldsymbol{x}), h(f^\tau(\boldsymbol{x})), h(f^{2\tau}(\boldsymbol{x})), ..., h(f^{(m-1)\tau}(\boldsymbol{x}))] \quad (2)$$

is an embedding when $m \geq 2n + 1$, where $n$ is the dimension of the manifold $\boldsymbol{M}$ of the phase space in which evolves the dynamics of the system. This means that interesting geometrical and dynamical characteristics of the underlying dynamics in the original phase space are preserved invariably in the reconstructed space as well.

Let $\boldsymbol{X}_r = \boldsymbol{\Phi}^{(t)}(\boldsymbol{X})$ be the reconstructed phase space and $\boldsymbol{x}_r(t_i) = \boldsymbol{\Phi}(\boldsymbol{x}(t_i))$ the reconstructed trajectory for the embedding $\boldsymbol{\Phi}$. Then the dynamics evolved in the original phase space is topologically equivalent to its mirror dynamical flow in the reconstructed phase space $\boldsymbol{X}_r$ according to

$$f_r^t(\boldsymbol{x}_r) = \Phi(x) \circ f^t(\boldsymbol{x}) \circ \Phi^{-1}(\boldsymbol{x}_r). \quad (3)$$

In other words, the embedding $\boldsymbol{\Phi}$ is a diffeomorphism which takes the orbits $f^t(\boldsymbol{x}_r)$ of the original phase space to the orbits in the reconstructed phase in such a way as to preserve their orientation and other topological characteristics as eigenvalues, Lyapunov exponents or dimensions of the attractors. According to the above theory, in the reconstructed phase space we can estimate geometrical characteristics as dimensions, which correspond to the degrees of freedom of the underlying dynamics of the experimental time series, as well as dynamical characteristics as Lyapunov exponents, mutual information and predictors (Pavlos et al., 1999a, b). Moreover, it is shown elsewhere that the method of reconstructed phase space conserves its significance even when the observed signal is derived by a stochastic process (Argyris et al., 1998; Pavlos et al., 1999c).

### 2.3 Correlation dimension

The theoretical concepts described above permit us to use experimental time series in order to extract useful geometric characteristics, which provide information about the underlying dynamics. Such a characteristic is the correlation dimension $D$, defined as

$$D = \lim_{r \to 0} \frac{d[\ln C(r)]}{d[\ln(r)]}, \quad (4)$$

where $C(r)$ is the so-called correlation integral for a radius $r$ in the reconstructed phase space. When an attracting set exists, then $C(r)$ reveals a scaling profile

$$C(r) \sim r^d \qquad \text{for} \qquad r \to 0. \quad (5)$$

The correlation integral depends on the embedding dimension $m$ of the reconstructed phase space and is given by the following relation

$$C(r, m) = \frac{2}{N(N-1)} \sum_{i=1}^{N} \sum_{j=i+1}^{N} \Theta(r - \parallel \boldsymbol{x}(i) - \boldsymbol{x}(j) \parallel), \quad (6)$$
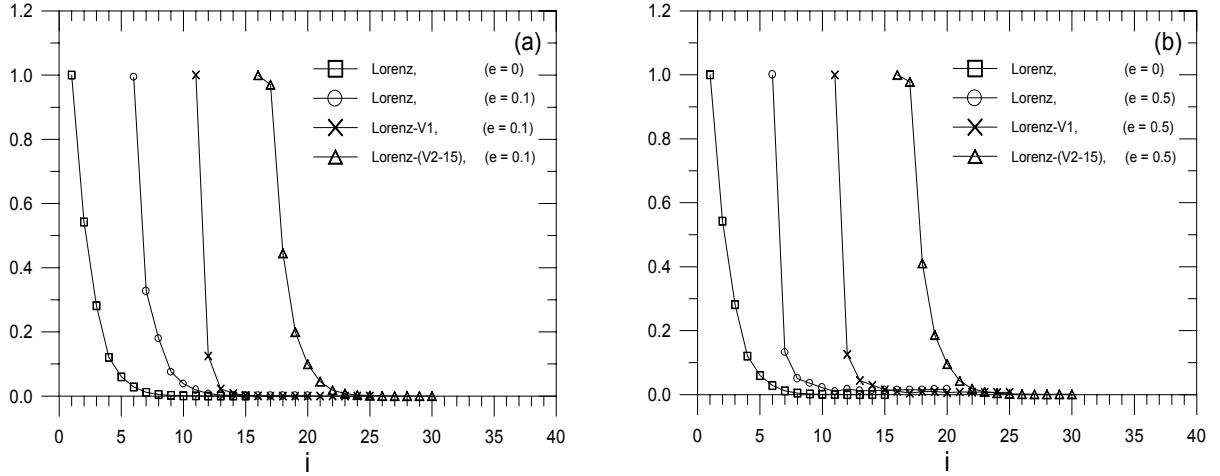
**Fig. 4. (a, b)** The spectra of the singular values $\sigma_i$, $i = 1 - 15$ corresponding to the purely deterministic $x(t)$ Lorenz signal, to the stochastic $x(t)$ Lorenz signal and its $V_1$, $V_{2-15}$ SVD components estimated for the levels $e = 0.1$ (37%) and $e = 0.5$ (39%) of the external noise perturbation.

where $\Theta(a) = 1$ if $a > 0$, $\Theta(a0) = 0$ if $a \leq 1$, and $N$ is the length of the time series. The scaling exponent $d(m)$ increases as we increase the embedding dimension $m$. When the time series is related to a low dimensional dynamical system then $d(m)$ saturates at a final value $D$ for a sufficiently large embedding dimension $m_0$. Theoretically, the value $m_0$ is the smallest integer larger than $D$, according to Ding et al. (1993), but in practice $m_0$ may attain larger values (Kugiumtzis, 1996), i.e. is an appropriate embedding may require a larger $m$ than the smallest integer larger than $D$.

For periodic attractors the correlation dimension $D$ becomes equal to the topological dimension $d$ of the manifold $M$, which includes the attractor. Usually for a strange attractor, $D$ obtains a fractal value.

When the slopes $d(m)$ of the correlation integrals reveal a plateau at low values of $r$ and the plateau converges for increasing $m$, then this is strong evidence for low dimensionality of the underlying dynamics for the observed signal. The stochastic component behaving as noise in the experimental time series, destroys the plateau and the saturation profile at low values of the radius $r$, and makes the derivation of reliable dimension estimates difficult (Pavlos et al., 1999c).

## 2.4 Singular value analysis (SVD) and SVD reconstructed components of the original time series

Singular value analysis has been proven to be a strong and effective method for modern time series analysis. It was used by Broomhead and King (1986) for the first time and comes from the generalized theory of information. In this study we use the above analysis in two cases: (i) as a time series filter and (ii) to decompose a time series in its SVD reconstructed components which can be used for the detection of the underlying dynamics. Singular value analysis is applied to the trajectory matrix which is constructed by an experimental time

series as follows:

$$X = \begin{bmatrix} x(t_1), & (t_1 + \tau), & \dots x(t_1 + (n-1)\tau) \\ x(t_2), & x(t_2 + \tau), & \dots x(t_2 + (n-1)\tau) \\ . & . & \dots \\ x(t_N), & x(t_N + \tau), & \dots x(t_N + (n-1)\tau) \end{bmatrix} = \begin{bmatrix} x_1^T \\ x_2^T \\ . \\ x_N^T \end{bmatrix}, (7)$$

where $x(t_i)$ is the observed time series and $t$ is the delay time for the phase space reconstruction. The rows of the trajectory matrix constitute the state vectors $x_i^T$ on the reconstructed trajectory in the embedding space $R^n$. As we have constructed $N$ state vectors in the embedding space $R^n$, the problem is how to use them in order to find a set of linearly independent vectors in $R^n$ which can satisfactorily describe the attracting manifold within the phase space according to the theoretical concepts of Sect. 2.1. These vectors constitute part of a complete orthonormal basis $\{e_i, i = 1, 2, ..n\}$ in $R^n$ and can be constructed as a linear combination of vectors on the reconstructed trajectory in $R^n$ by using the relation

$$s_i^T X = \sigma_i c_i^T. \quad (8)$$

According to singular value decomposition (SVD) theorem, it can be proved that the vectors $s_i$ and $c_i$ are eigenvectors of the structure matrix $\mathbf{XX}^T$ and the covariance matrix $\mathbf{X}^T\mathbf{X}$ of the trajectory, according to the relations

$$\mathbf{XX}^T s_i = \sigma_i^2 s_i, \qquad \mathbf{X}_T \mathbf{X} c_i = \sigma_i^2 c_i, \quad (9)$$

(see Brogan, 1982). The vectors $s_i$ , $c_i$ are the singular vectors of $X$, and $\sigma_i$ are its singular values, while the SVD analysis of $X$ can be written as

$$\mathbf{X} = \mathbf{S\Sigma C}^T, \quad (10)$$

where $S = [s_1, s_2, ...s_n]$, $C = [c_1, c_2, ...c_n]$ and $\Sigma = \text{diag}[\sigma_1, \sigma_2, ...\sigma_n]$. The singular values are assumed to obey the ordering $\sigma_{\geq}\sigma_2 \geq ... \geq \sigma_n \geq 0$ is assumed. It is also known from the SVD theorem that the non-zero eigenvalues

of the structure matrix are equal the to non-zero eigenvalues of the covariance matrix. This means that if $n'$ (where $n' \geq n$) is the number of the non-zero eigenvalues, then rank $\boldsymbol{X}\boldsymbol{X}^T$ = rank $\boldsymbol{X}^T\boldsymbol{X} = n'$. It is obvious that the n'-dimensional subspace of $R_N$ spanned by $\{\boldsymbol{s}_i, i = 1, 2, ...n'\}$ is mirrored to the basis vector $\boldsymbol{c}_i$, which can be found as the linear combination of the delay vectors by using the eigenvectors $\boldsymbol{s}_i$ according to Eq. (8). The complementary subspace spanned by the set $\{\boldsymbol{s}_i, i = n', 2, ...N\}$ is mirrored to the origin of the embedding space $R^n$ according to the same relation (8) i.e. the number of the independent eigenvectors $\boldsymbol{c}_i$ that are sufficient for the description of the underlying dynamics is equal to the number $n'$ of the non-zero singular values $\sigma_i$ of the trajectory matrix. The same number $n'$ corresponds to the dimensionality of the subspace containing the attracting manifold. The trajectory can be described on the new basis $\{\boldsymbol{c}_i, i = 1, 2, ...n\}$ by the trajectory matrix projected on the basis $\{\boldsymbol{c}_i\}$ given by the product $\boldsymbol{X}\boldsymbol{C}$ of the old trajectory matrix $\boldsymbol{X}$ and the matrix $\boldsymbol{C}$ of the eigenvectors $\{\boldsymbol{c}_i\}$. The new trajectory matrix $\boldsymbol{X}\boldsymbol{C}$ is described by the relation

$$(\boldsymbol{X}\boldsymbol{C})^T(\boldsymbol{X}\boldsymbol{C}) = \Sigma^2. \tag{11}$$

This relation corresponds to the diagonalization of the new covariance matrix so that the components of the trajectory are uncorrelated in the basis $\{\boldsymbol{c}_i\}$. Also, from the same relation (11) we conclude that each eigenvalue $\sigma_i^2$ is the mean square projection of the trajectory on the corresponding $\boldsymbol{c}_i$. Thus, the spectrum $\{\sigma_i^2\}$ includes information about the expansion of the trajectory in the directions $\boldsymbol{c}_i$ as it evolves in the reconstructed phase space. This phase space, explored by the trajectory, corresponds – on the average – to an $n$-dimensional ellipsoid for which $\{\boldsymbol{c}_i\}$ give the directions and $\{\boldsymbol{\sigma}_i\}$ the lengths of its principal axes in the subspace spanned by eigenvectors $\{\boldsymbol{c}_i\}$ corresponding to non-zero eigenvalues. However, when the system is perturbed by external noise or deterministic external input, then the trajectory begins to be diffused in directions corresponding to zero eigenvalues where the external perturbation dominates. As we show in the following, the replacement of the old trajectory matrix $\boldsymbol{X}$ with the new $\boldsymbol{X}\boldsymbol{C}$ works as a linear low pass filter for the entire trajectory. Moreover, the SVD analysis permits one to reconstruct the original trajectory matrix by using the $\boldsymbol{X}\boldsymbol{C}$ matrix as follows

$$\boldsymbol{X} = \sum_{i=1}^{n}(\boldsymbol{X}\boldsymbol{c}_i)\boldsymbol{c}_i^T. \tag{12}$$

The part of the trajectory matrix which contains all the information about the deterministic trajectory, as it can be extracted by observations, corresponds to the reduced matrix

$$\boldsymbol{X} = \sum_{i=1}^{n'}(\boldsymbol{X}\boldsymbol{c}_i)\boldsymbol{c}_i^T, \tag{13}$$

which is obtained by summing only with respect to eigenvectors $\boldsymbol{c}_i$ with non-zero eigenvalues. From the relation (12) we
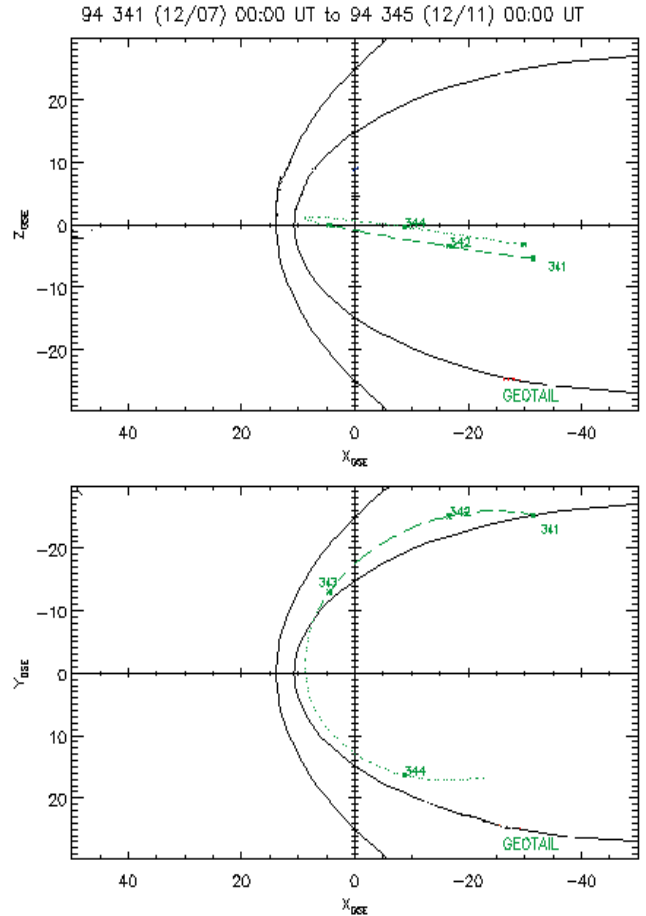


**Fig. 5.** Geotail orbit during the time interval 94, 341, 00:00 UT to 94, 345, 00:00 UT. During the time interval 341, 00:00 UT to 342, 12:00 UT the spacecraft moves in the dawn magnetosheath while it remains near the magnetopause and the low latitude boundary layer region of the magnetosphere.

can reconstruct the original time series $x(t)$ by using $n$ new time series $V(t_i)$ according to the relation

$$x(t) = \sum_{i=1}^{n} V_i(t), \tag{14}$$

where every $V_i(t)$ is given by the first column of the matrix $(\boldsymbol{X}\boldsymbol{c}_i)\boldsymbol{c}_i^T$. The $V_i(t)$ time series are known as SVD reconstructed components (Elsner and Tsonis, 1996). This is a kind of $n$-dimensional spectral analysis of a time series.

The new time series $V_i(t)$ constitute the reconstructed time series components of the SVD spectrum, corresponding to the spectrum of the singular vectors $\boldsymbol{c}_i$. The dependence of SVD analysis upon the existence of external noise is described by Broomhead and King (1986) for white noise and by Elsner and Tsonis (1996) for coloured noise. In the case of white noise the singular values $\{\overline{\sigma}_i\}$ of $X$ are shifted uniformly according to the relation

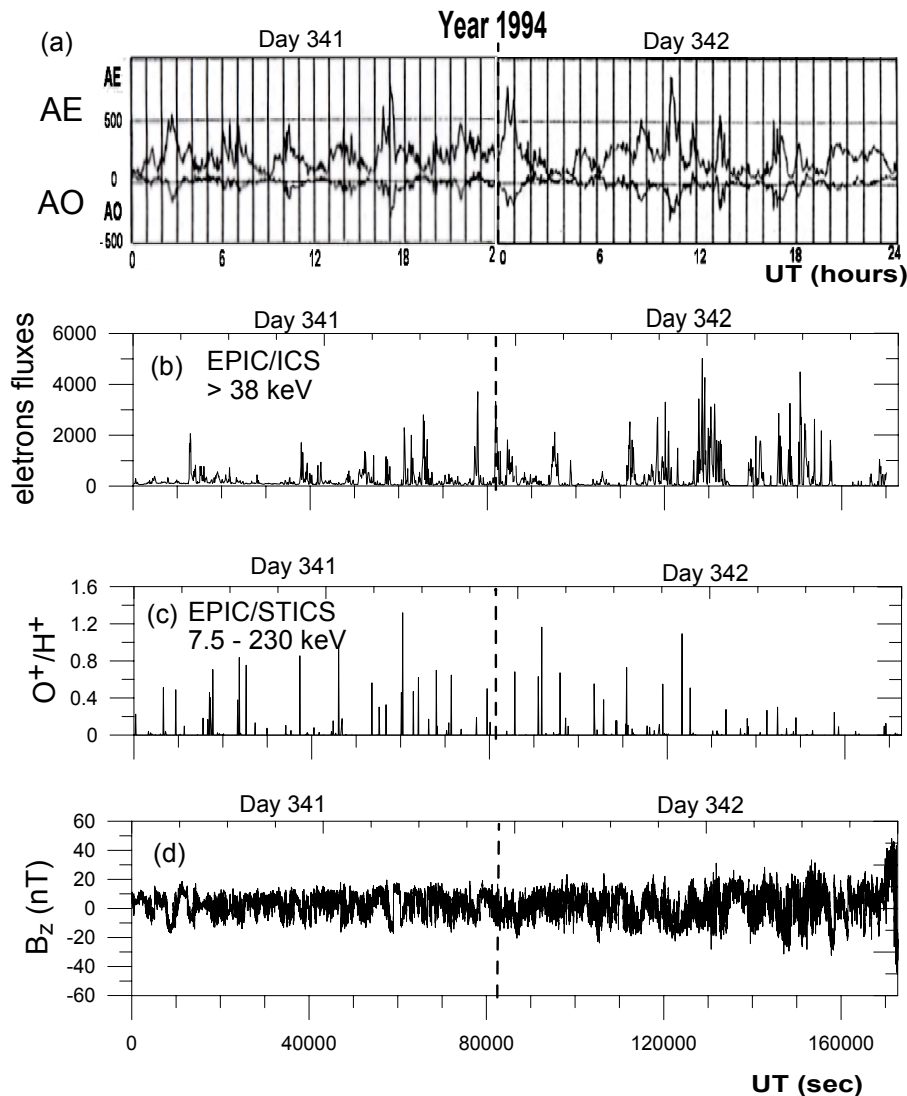$$\sigma_i^2 = \overline{\sigma}_i^2 + \langle\xi^2\rangle, \tag{15}$$

**Fig. 6.** From top to bottom, **(a)** $AE$ index measurements with one minute resolution, **(b)** the energetic $>38\,\text{keV}$ electrons (second panel), **(c)** the ratio $O^+/H^+$ (third panel) and **(d)** the $B_z$ component (fourth panel).

where $\overline{\sigma}_i$ are the singular values of the unperturbed signal and $\langle \xi^2 \rangle$ the perturbation of the external noise. Relation (15) indicates that, in the simple case of white noise the existence of a non-zero constant background or noise floor in the spectrum $\{\sigma_1\}$ can be used to distinguish the deterministic component. In this way we can obtain the deterministic component of the observed time series

$$X_d = \sum_{\sigma_i)\text{noise}} ((Xc)_i)c_i^T \qquad (16)$$

by using only singular values $\sigma_i$ greater than the noise floor. In addition, the relation (15) indicates that in the case of white noise the perturbation of the singular values $\sigma_i$ is independent of them. In contrast, as we show in the following, in the case of coloured noise the perturbation of the singular values is much stronger for the first singular value $\{\sigma_1\}$ than the others. This result may be expected as

the coloured noise includes finite dimensional determinism while the white noise includes an infinite dimensional signal. The above difference between white and coloured noise is significant because it makes the SVD analysis suitable for the discrimination between different dynamical components of the original signal.

### 2.5 Application of the SVD analysis in the deterministic and stochastic Lorenz system

In this section we apply the SVD analysis at the Lorenz system perturbed by external additive colored noise. The external colored noise is obtained by the equation

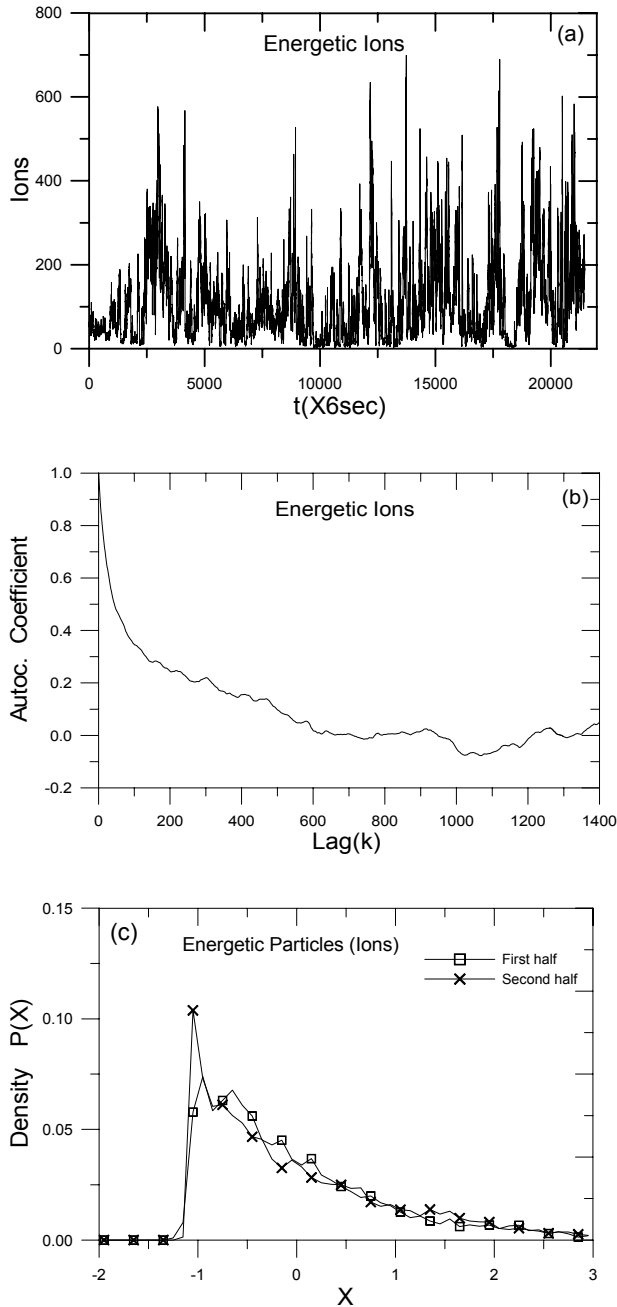$$X(t_i) = \sum_{k=1}^{M/2} C_k \cos(\omega_k t_i + \varphi_k), \quad i = 1, ..., M, \qquad (17)$$

**Fig. 7. (a)** Measurements of the magnetospheric energetic ions with six seconds time resolution during the days 7–8 December (day 341, 00:00 UT to day 342, 12:00 UT), 1994. The bursting character of the energetic ions is obvious and indicates the strong coupling of the magnetosphere with the solar wind. **(b)** The autocorrelation coefficient for the first 1400 units of the lag indicates two different processes. The first corresponds to an abrupt decay of autocorrelation coefficient and the second to a slow decay. **(c)** Amplitude distribution for the first and second half of the magnetospheric energetic ions time series. It is apparent the stationarity of the time series.

where the phases $\varphi_k$ are randomly distributed in the interval $[0, 2\pi]$, and $C_k$ are constants related to the power spectrum

$P(\omega_k)$ by

$$C_k = [P(\omega_k)\Delta\omega]^{1/2}. \tag{18}$$

As we have mentioned in Sect. 2.1 these random time series have a power spectra $P(\omega)$ of the form $\omega^{-\alpha}$ and show low dimensional fractality, with correlation dimension $D$ related through the relation $D = 2/(\alpha - 1)$, according to Osborne and Provenzale (1989). In this section we use two levels of coloured noise corresponding to the percentages 37% ($e = 0.1$) and 185% ($e = 0.5$), according to equation

$$x(t) = x_L(t) + ex_{cn}(t), \tag{19}$$

where the time series $x_{cn}(t)$ was constructed to have mean value of 38 and a standard deviation of 47.

Figure 2a shows the stochastic $x$-Lorenz time series including 37% of external coloured noise. Figure 2b shows the first SVD component $V_1$ of the stochastic signal described in Fig. 2a. The SVD reconstructed components $V_4$ and $V_{2-15}$ are shown in Figs. 2c–d. The component $V_{2-15}$ corresponds to the sum $\sum V_i, i = 2 - 15$ and approximates the original time series (shown in Fig. 2a), while the component $V_1$ approximates the typical profile of a nonstationary coloured noise. The component $V_4$ includes noticeable information contained in the original signal according to Fig. 2a. Figures 2e–h present the corresponding slopes of the correlation integrals estimated for the time series of Figs. 2a–d. The slopes shown in Fig. 2e correspond to the original stochastic signal, and the slopes shown in Figs. 2f–h correspond to the slopes of the SVD components $V_1$, $V_4$ and $V_{2-15}$ of the original Lorenz coloured noise stochastic signal. The slopes of the original stochastic signal (Fig. 2e) reveal a small tendency for scaling and saturation of the scaling exponents at the values $D = 3 - 4$ in the range $\Delta \ln r = 1 - 3$ of the distance $r$ in the reconstructed phase space. However, this weak profile of scaling and saturation is entirely destroyed passing to the $V_1$ component, as seen in Fig. 2f.

A significant profile of scaling and low value saturation of the slopes reappears passing to the next SVD components $V_4$ and $V_{2-15}$, as we can see in Figs. 2g–h. The correlation dimension estimated for the time series $V_4$ and $V_{2-15}$ was found to be $\sim 2.5$. This value does not differ significantly from the correlation dimension of the purely deterministic Lorenz system. The results discussed above reveal three significant characteristics concerning the coloured noise:

(a) The coloured noise causes a significant elevation of the saturation value $D$ of the scaling exponents.

(b) The coloured noise perturbation is absorbed mainly by the $V_1$ SVD component destroying the scaling and the low value saturation profile of the slopes corresponding to the $V_1$ SVD component.

(c) The higher SVD components ($V_4$, $V_{2-15}$) absorb a much lower percentage of the noise. The correlation dimension of these SVD components does not differ significantly from the correlation dimension of the purely deterministic system.

**Table 1.** This Table presents the ratio $\sigma_2/\sigma_1$ estimated for the original Lorenz system, the stochastic (coloured noise) Lorenz system and the SVD components of the stochastic Lorenz system

| | Lorenz with coloured noise | | | | | |
|---|---|---|---|---|---|---|
| | $\sigma_2/\sigma_1$ | e | Noise % | $\sigma_2/\sigma_1$ | e | Noise % | $\sigma_2/\sigma_1$ |
| Lorenz | 0.54 | 0.1 | 37 | 0.33 | 0.5 | 185 | 0.04 |
| Lorenz-$V_1$ | 0.68 | 0.1 | 37 | 0.12 | 0.5 | 185 | 0.02 |
| Lorenz-$(V_{2-15})$ | 0.63 | 0.1 | 37 | 0.45 | 0.5 | 185 | 0.41 |

**Table 2.** This Table presents the ratio $\sigma_2/\sigma_1$ estimated for the original Lorenz system, the stochastic (white noise) Lorenz system and the SVD components of the stochastic Lorenz system

| | Lorenz with white noise | | | | | |
|---|---|---|---|---|---|---|
| | $\sigma_2/\sigma_1$ | e | Noise % | $\sigma_2/\sigma_1$ | e | Noise % | $\sigma_2/\sigma_1$ |
| Lorenz | 0.54 | 1 | 7.8 | 0.50 | 5 | 39 | 0.50 |
| Lorenz-$V_1$ | 0.68 | 1 | 7.8 | 0.45 | 5 | 39 | 0.45 |
| Lorenz-$(V_{2-15})$ | 0.63 | 1 | 7.8 | 0.47 | 5 | 39 | 0.47 |

The above characteristics reveal a strong difference between the behaviour of the coloured and white noise as we perturb a dynamical system concerning the correlation dimension. As we have shown elsewhere (Athanasiu and Pavlos, 2001), the white noise leaves invariant the correlation dimension passing from the original stochastic signal to its SVD components. However, the coloured noise leaves invariant only the high SVD components. In the following we present results concerning the autocorrelation coefficient and the singular value spectrum of the Lorenz system perturbed by external additive coloured noise. Figure 3a shows the autocorrelation coefficient estimated for the original ($e = 0$) Lorenz system and for the Lorenz system perturbed by external coloured noise corresponding to amplitudes ($e = 0.1, e = 0.5$). In the same figure we present the autocorrelation coefficient of the first SVD component $V_1$ of the original stochastic signal. It is important to notice that there is a clear difference between the original signal and its $V_1$ SVD component concerning the decorrelation time. This characteristic is similar for the coloured and white noise. On the other hand, the behaviour of the coloured noise is different from that of the white noise passing from one level of noise to another for both cases of the original signal and its $V_1$ component, i.e. in the case of the coloured noise the decorrelation time increases as we increase the amplitude of the external perturbation for both the original signal and its first SVD component $V_1$. This result is in contrast to the behaviour of the white noise perturbation, as it has been shown in Athanasiu and Pavlos (2001). The autocorrelation coefficients for the next SVD components ($V_4, V_{2-15}$) of the original stochastic signal are shown in Figs. 3b–c. These figures reveal similar behaviour between the colored noise and the white noise, as

the decorrelation time of the ($V_4, V_{2-15}$) SVD components remains invariant, passing from weak to strong external perturbation.

Figures 4a–b show the singular value spectrum estimated for the coloured noise stochastic Lorenz system and its SVD components ($V_1, V_{2-15}$). Figure 4a corresponds to the first level ($e = 0.1$) of the coloured noise perturbation and Fig. 4b to the second level ($e = 0.5$). As it is concluded by these figures the coloured noise destroys the normal character of the nontrivial singular values for the stochastic signal and its $V_1$ SVD component, causing the ratio of the second to first eigenvalue $\sigma_2/\sigma_1$ to decrease significantly, passing from the purely deterministic to the stochastic signal. However, this effect is not observed for the $V_{2-15}$ SVD component. Table 1 presents the ratio $\sigma_2/\sigma_1$ estimated for the original Lorenz system, the stochastic (coloured noise) Lorenz system and the SVD components of the stochastic Lorenz system. For both levels of perturbation ($e = 0.1, 0.5$) the ratio decreases, passing from the purely deterministic system to the corresponding stochastic system and the $V_1$ component of the stochastic system. On the contrary, the ratio $\sigma_2/\sigma_1$ increases, passing from the $V_1$ to the $V_{2-15}$ SVD component obtaining almost the value of $\sigma_2/\sigma_1$ estimated for the purely deterministic Lorenz system. Table 2 is similar to Table 1, corresponding to the case of the white noise perturbation Lorenz system. This table shows that the ratio $\sigma_2/\sigma_1$ is almost invariant, passing from the purely deterministic signal to the corresponding stochastic signal and the SVD components of the second. The above results reveal that as in the case of the correlation dimension and the autocorrelation coefficient, the behaviour of the colored noise is strongly discriminated from the white noise and in the case of the singu-
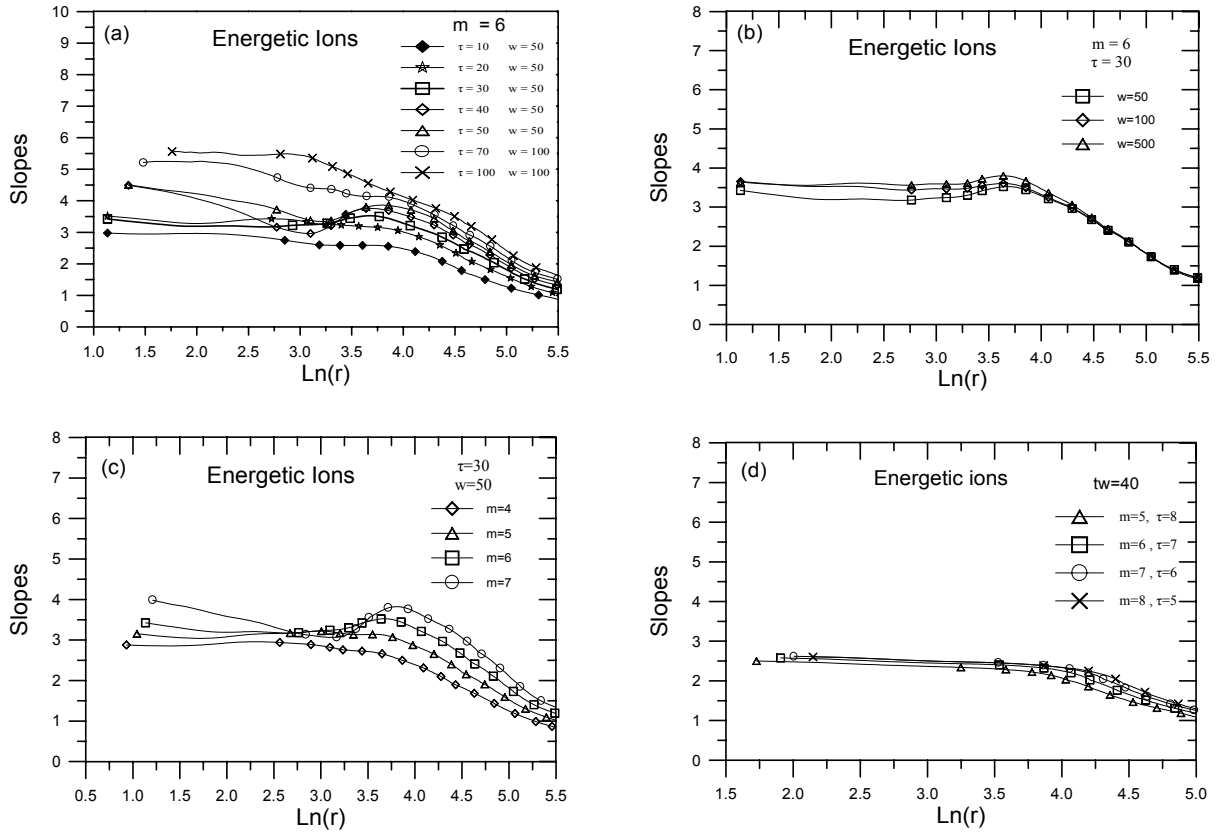
**Fig. 8.** (a) The slope of the correlation integral as a function of the radius $r$ estimated for embedding $m = 6$, delay time $\tau = 10 - 100$ units of the sampling time and Theiler's parameter $w = 50, 100$. For delay time $\tau = 20 - 50$ we observe the best scaling. (b) The same as (a) but with delay $\tau = 30$ and $w = 5500$, showing that there is no significant change of the slopes. (c) The same as (a) but with $\tau = 30$, $w = 500$ and a embedding dimension $m = 4 - 7$. (d) The same as (c) estimated by using the SVD filtering of the original signal for window length $\tau_w$, $w = 50$ and independent trajectory matrices for every embedding.

lar value spectrum as well.

### 2.6 The method of the false nearest neighbours in the estimation of the dynamical degrees of freedom

Besides the correlation dimension, the method of false nearest neighbours can also give an estimation of the smallest value that is appropriate for the embedding dimension $m_0$. When the trajectory of the system is reconstructed in a space of low dimensionality, then it is possible to have self-crossings which give rise to false neighbours state vectors. This is gradually improved as the embedding dimension is increased, and for a large enough embedding dimension $m_0$ false crossings and false neighbours disappear. Let $\boldsymbol{x}(j)$ be the nearest point to $\boldsymbol{x}(i)$ for an embedding dimension $m$. Then their distance is given by

$$r_m^2(i, j) =$$

$$[x(i) - x(j)]^2 + \ldots + [x(i + (m-1)\tau) - x(j + (m-1)\tau)]^2. \quad (20)$$

Passing from the $m$ to $m + 1$ embedding dimension this distance takes the form

$$r_{m+1}^2(i, j) = r_m^2(i, j) + [x(i + m\tau) - x(j + m\tau)]^2. \quad (21)$$

Then if

$$\frac{|x(i + m\tau) - x(j + m\tau)|}{r_m} > R_T, \quad (22)$$

the nearest neighbours at time $i$ are declared as false (Abarbanel et al., 1993). The threshold value $R_T$ is estimated to be in the range $10 \leq R_T \leq 50$. According to this criterion, as the embedding dimension $m$ increases to a characteristic value $m_0$, the percent of false nearest neighbours may drop to zero. If this is actually observed for a time series, then it yields a positive indication of the existence of low dimensional dynamics underlying the observed signal.

### 2.7 The method of surrogate data

According to the relation (5), the scaling properties of the correlation integral as $r \to 0$ and the saturation of the scaling exponent $d(m) \to D$ as $m$ increases are necessary conditions for the existence of low dimensional dynamics underlying the experimental time series. However, it has been shown that these conditions are not sufficient in order to conclude low dimensional dynamics from experimental time series with broad-band power spectrum, as they can also be satisfied by stochastic systems (Osborne and Provenzale, 1989;
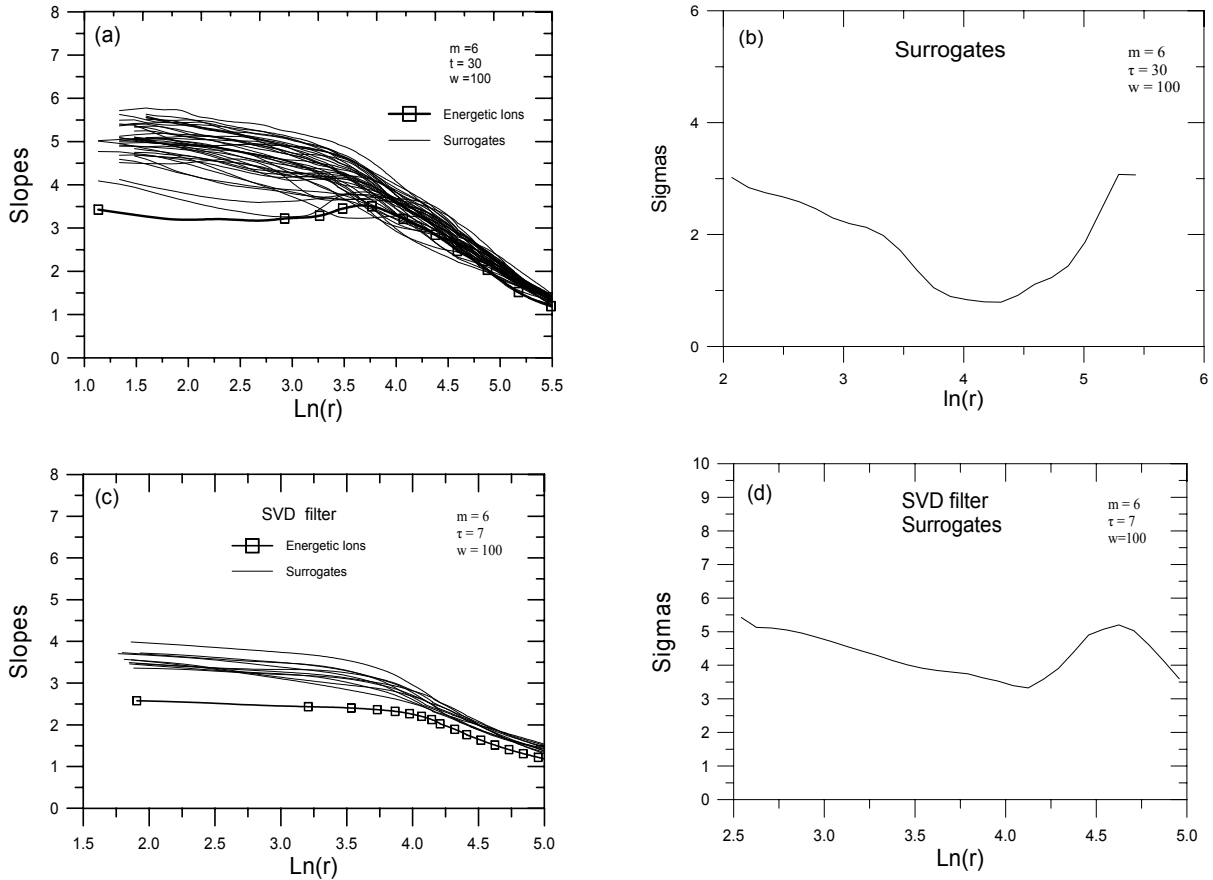
**Fig. 9.** **(a)** Slopes of the correlation integrals estimated for the original signal and its first 30 surrogate data as a function of $\ln(r)$. **(b)** The significance of the statistics as a function of $\ln(r)$, shown in (a). **(c, d)** The same as (a, b) but SVD analysis was used.

Provenzale et al., 1991). Moreover, according to Theiler (1991), the concept of low correlation dimension (fractal or integer) can be applied to time series in two distinct ways. The first one indicates the number of degrees of freedom in the underlying dynamics, and the second quantifies the self-affinity or "crinkliness" of the trajectory through the phase space. In the first case, the scaling and saturation profile are caused by the recurrent character of the reconstructed trajectory, i.e. by uncorrelated in "time" and correlated in "space" state points. In the second case, they are caused by time correlated state points that are uncorrelated in space. In order to discriminate between the two cases, known as dynamic and geometric low dimensionality, we restrict the sum in Eq. (6) to pairs $(x(i), x(j))$ with $|i - j| > w$, where the Theiler parameter $w$ is larger than the decorrelation time of the time series.

When low dimensionality is persistent as a dynamic characteristic after the application of Theiler's criterion, then we have to decide first between linearity and nonlinearity and second between chaoticity and pure stochasticity. By the term chaoticity we mean the case where the deterministic component of the process is prevalent and reveals low dimensional chaos. For a stochastic process, the deterministic component may correspond to low dimensionality and even

nonlinear and chaotic dynamics, but its effect can hardly be observed as the process is driven mainly by noise. Therefore, we focus here on the solution of the first problem, i.e. determining whether the magnetospheric ions' time series is linear or nonlinear. This is done by following the method of "surrogate" data (Theiler et al., 1992a, b).

The method of "surrogate" data includes the generation of an ensemble of data sets which are consistent to a null hypothesis. According to Theiler (1992a), the first type of null hypothesis is the linearly correlated noise which mimics the original time series in terms of the autocorrelation function, variance and mean. The second and more general null hypothesis takes into account that the observed time series may be a nonlinear monotonic static distortion of a stochastic signal.

Every Gaussian process is linear, while a non-Gaussian process can be linear or nonlinear. An experimental time series may show nonlinearity in terms of a non-Gaussian distribution, which may be due to a nonlinear transformation of the linear underlying dynamics. In this case, the generated "nonlinear" surrogate data mimic the original time series $x(i)$ in terms of the autocorrelation function and the probability density function $p(x)$. It is always possible for a nonperiodic time series of finite length to be a particular realisation of a

noise process or of a low-dimensional deterministic process. Therefore, it is a statistical problem to distinguish between a nonlinear deterministic process and a linear stochastic process. For this purpose we use as discriminating statistic a quantity $Q$ derived by a method sensitive to nonlinearity, as the correlation dimension estimation. The discriminating statistic $Q$ is calculated for the original and the surrogate data, and the null hypothesis is verified or rejected according to the value of "sigmas" $S$

$$S = \frac{\mu_{obs} - \mu_{sur}}{\sigma_{sur}}, \qquad (23)$$

where $\mu_{sur}$ and $\sigma_{sur}$ is the mean and the standard deviation of $Q$ on the surrogate data, and $\mu_{obs}$ is the mean of $Q$ on the original data. For a single time series, $\mu_{obs}$ is the single $Q$ value (Theiler et al., 1992a).

The significance of the statistics is a dimensionless quantity, but we follow here the common parlance and report it in terms of the units of $S$ "sigmas". When $S$ takes values higher than 2–3, then the probability that the observed time series does not belong to the same family with its surrogate data is higher than 0.95–0.99, correspondingly.

For testing the second more general null hypothesis described above we follow Theiler's algorithm (Theiler, 1992a), as well as Schreiber and Schmitz's algorithm (Schreiber and Schmitz, 1996). Both algorithms create stochastic signals which have the same autocorrelation function and amplitude distribution as the original time series.

According to Theiler's algorithm, a white Gaussian noise is first reordered to match the rank of the original time series (this is to make the original time series Gaussian). Then the phases of this signal are randomized (to destroy any possible nonlinear structure). Finally, the original signal is reordered to match the rank of the above constructed coloured noise (to regain the original amplitude distribution). The derived shuffled time series is the surrogate time series.

The algorithm of Theiler was improved by Schreiber and Schmitz by a simple iteration scheme, in order to strengthen the ability of the surrogate data to fit more exactly the autocorrelation function and the power spectrum of the original time series. The procedure starts with a white noise signal, in which the Fourier amplitudes are replaced by the corresponding amplitudes of the original data. The rank order of the derived stochastic signal is used to reorder the original time series. By doing this the matching of amplitude distribution is succeeded, but the matching of power spectrum achieved in the first step is altered. Therefore, the process obtained in the two steps is repeated several times until the change in the matching of power spectrum is sufficiently small. In the analysis of our data the improved algorithm of Schreiber and Schmitz is used.

## 3   Data analysis and results

It is known that protons or heavy ions as $O^{6+}$ could be accelerated by Fermi acceleration at the Earth's bow shock (Ipavich et al., 1981; Freeman and Parks, 2000). However, low charge state heavy ions are thought to be coming from the Earth's ionosphere and accelerated in the magnetotail (Kirsch et al., 1984; Pavlos et al., 1985; Eastman and Christon, 1995; Anagnostopoulos et al., 1986, 1998; Sarafopoulos et al., 1999; Christon et al., 2000). Moreover, it is known that bursts of energetic electrons are caused only by acceleration in the Earth's magnetotail (Pavlos et al., 1985; Anagnostopoulos et al., 1986; Sarafopoulos et al., 2000). In this work we study an extendend time series of energetic ions as they were observed at the dawn magnetosheath of the Earth's magnetosphere. As we can see in Figs. 5a–b during the days 7–8 December (days 341–342), 1994, the spacecraft GEOTAIL moves in the down magnetosheath while it remains near the magnetopause and the low-latitude boundary layer (LLBL) region of the magnetosphere. Figure 6a shows the $AE$ index during the same period. The profile of the $AE$ index indicates strong magnetopsheric activity which could cause the acceleration of electrons, protons and low charge state heavy ions as $O^{6+}$. Figures 6b–c present energetic electron fluxes as well as $O^+$ fluxes, which obviously were accelerated at the Earth's magnetotail. Figure 6d shows the $B_z$ magnetic field measurements during the same period. The $B_z$ component changes continuously from negative to positive values, indicating the magnetic connection of the spacecraft's position and the Earth's magnetosphere. The magnetic connection of the spacecraft and magnetopshere can be also concluded by the existence of energetic electron bursts (see Fig. 6b). Sarafopoulos et al. have also determined energetic electrons and proton bursts during the same period, and they concluded their magnetopsheric origin (Sarafopoulos et al., 2000). These observations strongly support the hypothesis that the energetic ions observed during the same period at the dawn magnetosheath were produced at the Earth's magnetotail.

Figure 7a shows the measurements of the energetic ions (35–46.8 keV) as they were observed by the experiment EPIC/ICS during the days 7–8 December (day 341, 00:00 UT to day 342, 12:00 UT), 1994, at the dawn magnetosheath of the Earth's magnetosphere. This figure reveals strong and continuously repeatable bursts of energetic ions during ~36 h. As it was explained before, it is reasonable to suppose that these particles were accelerated in the inner magnetosphere during periods with a strong coupling of the magnetospheric system and the solar wind, simultaneously with strong bursts of electrons and $O^+$, as well as a clear enhancement of the $AE$ index. Therefore, it can be supposed that the dynamics of the energetic ions mirror the internal magnetospheric dynamics, similar to the $AE$ index during periods with a strong coupling of the magnetosphere and the solar wind (Pavlos et al., 1999c). The energetic particle differential fluxes are provided via the Energetic Particle and Ion Composition (EPIC) instrument of the GEOTAIL spacecraft, and essentially remained close to the ecliptic plane (Williams et al., 1994). The sampling time for the energetic ions analyzed here was 6 s.

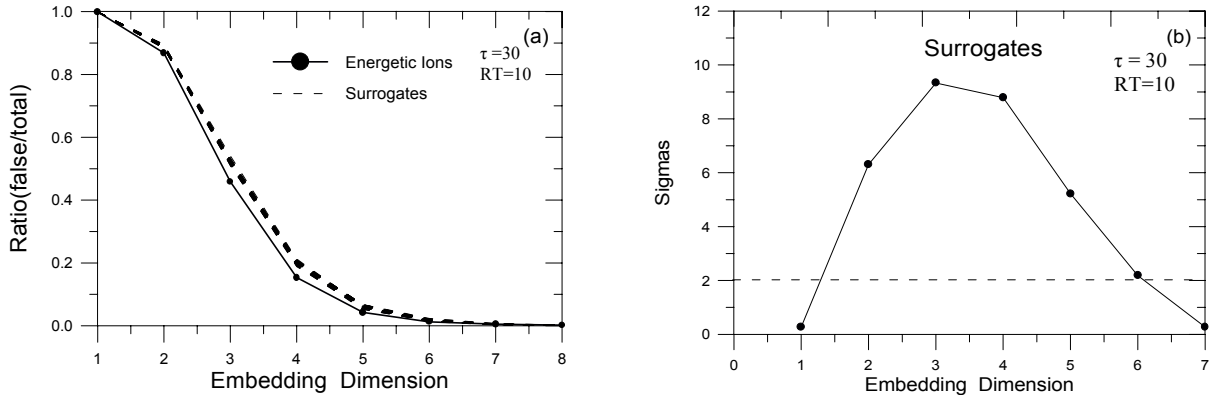The time series shown in Fig. 7a contains $N_T \cong 20\,000$

**Fig. 10. (a)** The ratio of the false to the total nearest neighbours for the original time series and its surrogate data as a function of $m$. For this estimation we used $\tau = 30$ and $R_T = 10$. **(b)** The significance of the statistics for the surrogate data.
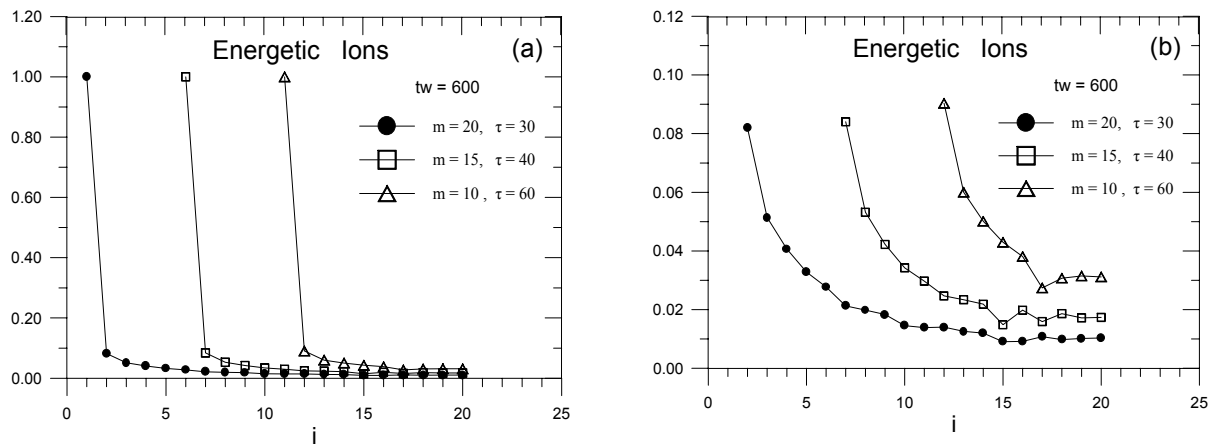


**Fig. 11. (a)** The spectra of singular values $\sigma_i$, with parameter $m = 10, 15, 20$, estimated for the energetic ions time series. **(b)** The same with (a) but discarding the first singular value.

data points. Figures 7b and c present the autocorrelation function and the amplitude distribution of the energetic ions' time series. The first figure reveals abrupt decorrelation of the signal during the first 150–200 units of lag time, which implies a broad-band spectrum. The second figure reveals that the distribution of the amplitudes is non-Gaussian, which under certain conditions (especially when the signal is ergodic) can lead to the possibility of nonlinearity existing in the signal. The nonlinearity can be dynamical or static, something which will be clarified in the following by the method of surrogate data. The random character of the energetic ions' time series is revealed by the decaying profile of the autocorrelation coefficient showing an abrupt decay during the first 100 units of the lag time and a slow, long decay afterwards. The general profile of the autocorrelation coefficient indicates two different physical processes: one corresponding to short decorrelation time (100 lags) and the other corresponding to long decorrelation time (1000 lags). The first process is assumed to be related to a low dimensional chaotic process, while the second corresponds to a coloured noise mechanism. Of course the abrupt decay (first kind of

process) cannot be explained solely as a consequence of a chaotic process, as it is possible to be caused by a static nonlinear distortion of a linear stochastic system. The stationarity of the time series is tested by estimating the amplitude distributions for the first and second half of the data set shown in Fig. 7a. In the same figure, except for the stationarity of energetic ions time series, the non-Gaussian character of the signal is also revealed. This indicates the possibility for nonlinearity in the signal and the underlying physical mechanism.

### 3.1 Correlation dimension

Figure 8a shows the slopes of the correlation integral estimated for the embedding dimension $m = 6$, different delay times ($\tau$) and different values of Theiler's parameter ($w$). For delays of 10–50 lags the slopes reveal a satisfactory scaling at low values of distance r in the reconstructed phase space. This result indicates the delay value time $\tau = 30 - 40$ as a suitable value for a reliable reconstruction of the phase space trajectory and the trajectory matrix **X**.
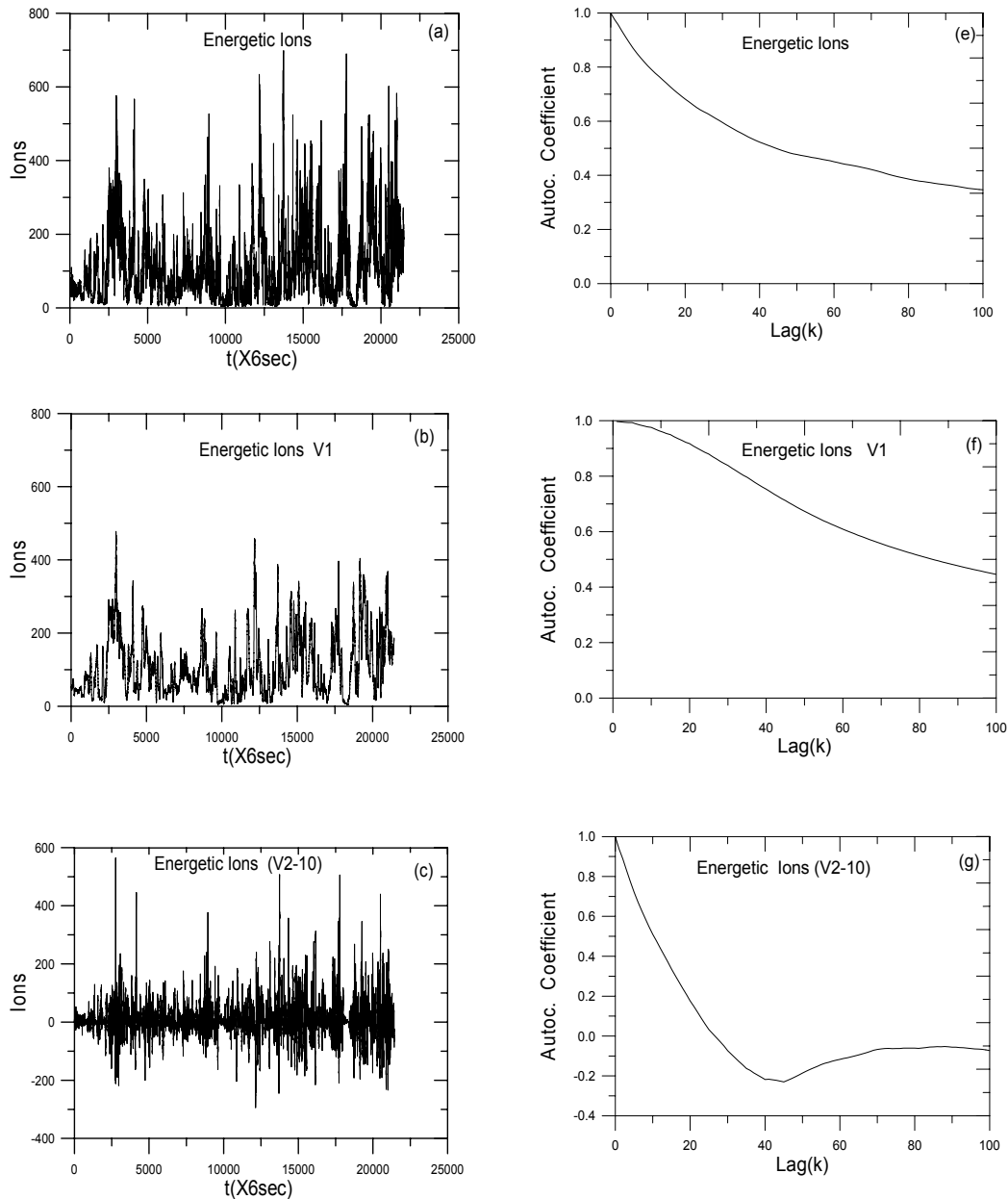
**Fig. 12. (a)** The magnetospheric energetic ions time series during the days 7–8 December 1994. **(b)** The time series corresponding to the $V_1$ component of the SVD analysis of the signal shown in (a). **(c)** The time series corresponding to the SVD reconstructed component $V_{2-10} = \sum V_i$, ($i = 2 - 10$), of the signal shown in (a). **(e, f, g)** The autocorrelation coefficient estimated for the signals shown in (a),(b),(c) respectively.

Figure 8b is similar to Fig. 8a but for different values of Theiler's parameter $w$. This figure indicates that the slope of the correlation integral remain almost invariant for $w > 500$. Figure 8c shows the slopes, of the correlation integral for different embedding dimensions ($m = 4 - 7$). It reveals a tendency for low value saturation of the slopes ($D \approx 3 - 4$), at the scaling region $\Delta ln(r) = 2.5 - 3.5$. However, the existence of external noise has destroyed substantially the scaling and the saturation profile of the slopes at smaller values of the distance ($r$). The dependence of the slopes of the correla-

tion integrals upon external perturbation has been described in the previous section, where it has been shown that the external noise perturbation destroys the slopes at small values of the distance ($r$) and leaves them invariant at higher values. Also, it has been shown that the coloured noise can raise the saturation value of the slopes by about 1–2 units. Contrary, the white noise leaves invariant the saturation value of the slopes. In order to exclude the perturbation of the slopes caused by external high dimensional stochasticity related to white or coloured noise, we use the new trajectory matrix **XC**

obtained by the SVD method and describe the trajectory on the basis of the singular vectors ($c_i$), as it was presented in Sect. 2.4.

Figure 8d presents the slopes estimated by using the new trajectory matrix **XC**. We can now notice that there is clear improvement of the scaling and saturation profiles. The observed saturation value $D \approx 2.5$ of the slopes indicates the low dimensionality of the physical process underlying the energetic ions' time series. Although the low value saturation of the slopes indicates the existence of dynamical low dimensionality in the underlying process, it is not helpful, however, in deciding upon stochasticity or chaoticity of the signal and the underlying dynamics. In order to exclude the linear stochasticity of the signal we use the method of surrogate data (described in Sect. 2.7).

Figure 9a shows the slopes of the surrogate data estimated for the embedding dimension $m = 6$ and it is compared with the corresponding slopes of the original time series. For the statistics we used forty independent surrogate signals. The significance of the statistics is shown in Fig. 9b. At the scaling region $\Delta ln(r) = 1.0 - 3.0$ of the distance ($r$) and the significance takes values higher than two sigmas. This indicates that the energetic ions' time series does not belong to the same family of the surrogate data and this happens with probability greater than 0.95, i.e. we can reject the null hypothesis with a confidence greater than 95%. Figures 9c and d are similar to Figs. 9a and b and correspond to the slopes obtained by the SVD trajectory matrix **XC**. Now the significance ($S$) stays at values $S = 3 - 5$ along the entire scaling region (Fig. 9d). This significance improves the confidence of discrimination between the original and the surrogate data to the value greater than 99%. Thus, the results discussed above support the concept of the dynamic nonlinearity and low dimensional chaos of the energetic ions' time series, excluding with high confidence the case of linear stochasticity, which can mimic dynamical nonlinearity and low dimensional chaos after a static nonlinear distortion.

## 3.2 False nearest neighbours

The ratio of the false to total neighbours was estimated according to the theoretical concepts presented in Sect. 2.6 for the energetic ions' time series, as well as for the two sets of surrogate data. Figure 10a shows these ratios for the ions' signal and the first ten series of surrogate data as a function of the embedding dimension. For the statistical comparison we have also used 40 independent signals of surrogate data. In both cases the ratio of false to total neighbours approaches zero for $m > 6 - 7$, indicating that there are 6 or 7 dynamical degrees of freedom of the underlying process. The significance of the statistical tests is presented in Fig. 10b as a function of the embedding dimension ($m$). The levels of significance are found to be $S = 5 - 10$ sigmas for the embedding dimension $m = 2 - 5$. This result indicates a strong possibility of discrimination between the original signal and the surrogate data, i.e. the null hypothesis can be rejected with a confidence greater than 99%. These results also support

strongly the concepts of low dimensionality and dynamical nonlinearity of the original signal excluding the hypothesis of the linear stochastic signal, which can mimic the characteristics of the observed energetic ions' signal after a static and nonlinear distortion.

## 3.3 Singular value spectrum

Figure 11a presents the normalized spectrum of the singular values estimated for embedding $m = 10 - 20$. For the estimation of the singular value spectrum we have followed the methods that appeared in the papers of Broomhead and King (1986), Albano et al. (1988), where they used a fixed window length $\tau_w$. According to Albano et al., the lower and upper limits for $\tau_w$ are based on the autocorrelation function and are proposed to be $\tau_c < \tau_w < 4\tau_c$, where $\tau_c$ is the correlation time defined as the time where the autocorrelation function is $1/e$. Here we use a fixed window length $\tau_w = 600$, while the delay time ($\tau$) and the embedding dimension $m$ are variable, according to the relation $\tau_w = m\tau$. As we can see in Fig. 11a, the first singular value $\sigma_1$ is much larger than the next ones $\sigma_i, i \geq 2$, which are pressed to the noise floor. This characteristic was also observed in the case of the Lorenz stochastic system, related to coloured noise perturbation and described in Sect. 2.5. As we show in the next subsections, the similarity of the energetic ions dynamics with the coloured noise stochasticity is a global characteristic. This indicates further that the dynamical process underlying the energetic ion time series must be perturbed by an external coloured noise process. Figure 11b shows the spectrum of singular values $\sigma_i, i \geq 2$. This figure reveals that by excluding the first singular value $\sigma_1$, we can obtain a normal spectrum with 6–7 nontrivial singular values above the noise floor. This result is similar to the result obtained by the method of false nearest neighbours and indicates 6–7 dynamical degrees of freedom corresponding to the magnetospheric process underlying the energetic ions' time series.

## 3.4 SVD spectrum of reconstructed components

In order to further understand the dynamical process underlying the energetic ions' time series, we study the spectrum of the SVD reconstructed components according to the theoretical concepts and results discussed in Sects. 2.4 and 2.5. Figure 12a–c show the time series corresponding to the observed energetic ions time series (Fig. 7a) and its $V_1$, $V_{2-10}$ SVD components. The component $V_{2-10}$ is computed by the following sum

$$V_{2-10} = \sum_{i=2}^{1} 0 V_i \tag{24}$$

of the $V_i, i = 2 - 10$ SVD components. The $V_1$ SVD component shown in Fig. 12b describes the low variation of the original time series, while the higher component $V_{2-10}$ (shown in Fig. 12c) includes the fast variation of the original signal. Figure 12e–g presents the corresponding autocorrelations coefficients of the time series shown in Fig. 12a–c. The
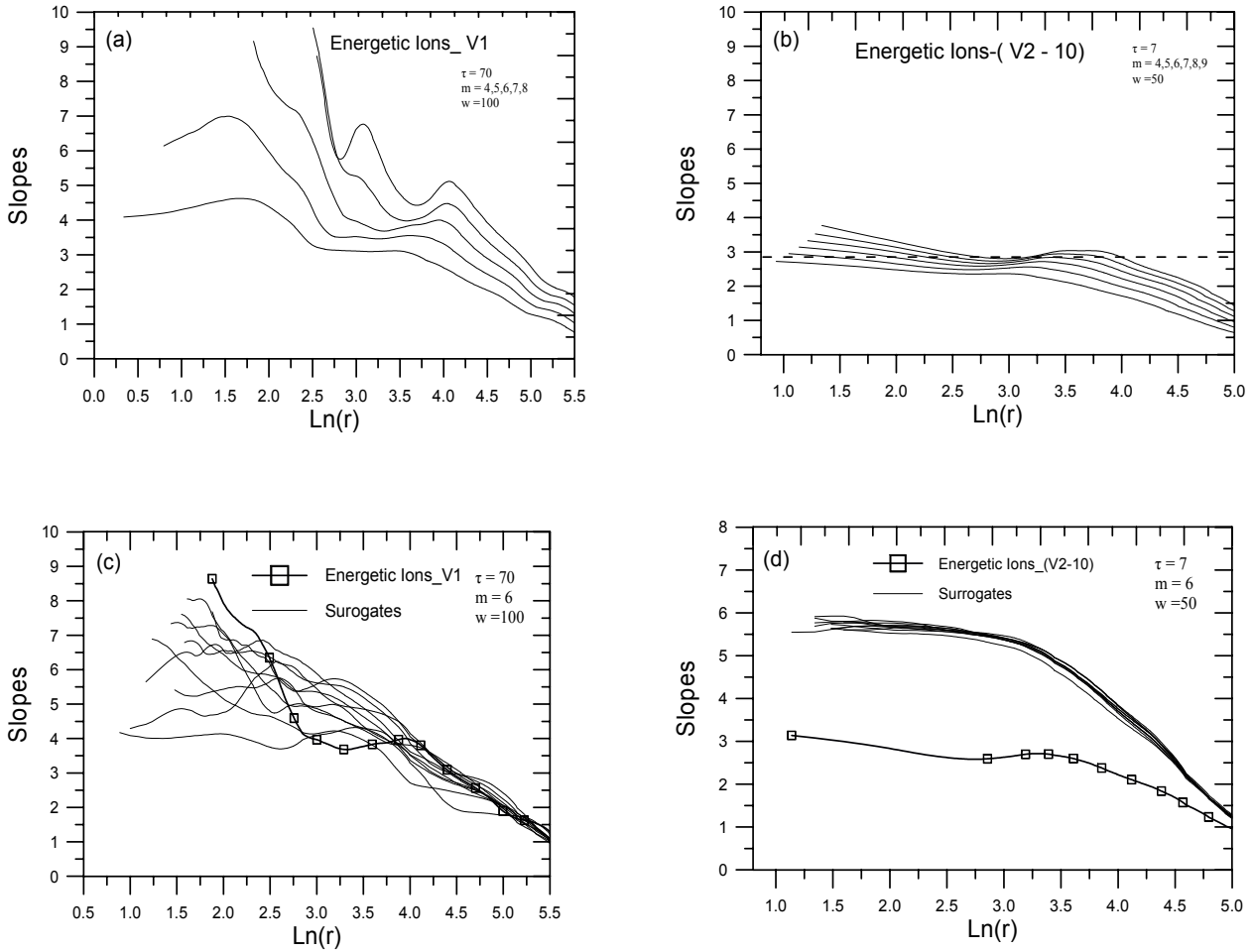
**Fig. 13.** (a) The slopes of the correlation integrals estimated for the $V_1$ SVD reconstructed component of the energetic ions time series for $m = 4 - 8$, $\tau = 70$ and Theiler's parameter $w = 100$. (b) The same as (a) but for the SVD reconstructed component $V_{2-10} = \sum V_i$, ($i = 2 - 10$) with parameters $m = 4 - 9$, $t = 7$, $w = 500$. (c) The same as (a) but for the $V_1$ SVD reconstructed component and its surrogate data with parameters $m = 6$, $t = 70$, $w = 100$. (d) The same as (b) but for the $V_{2-10}$ SVD reconstructed component and its surrogate data with parameters $m = 6$, $\tau = 70$, $w = 50$.
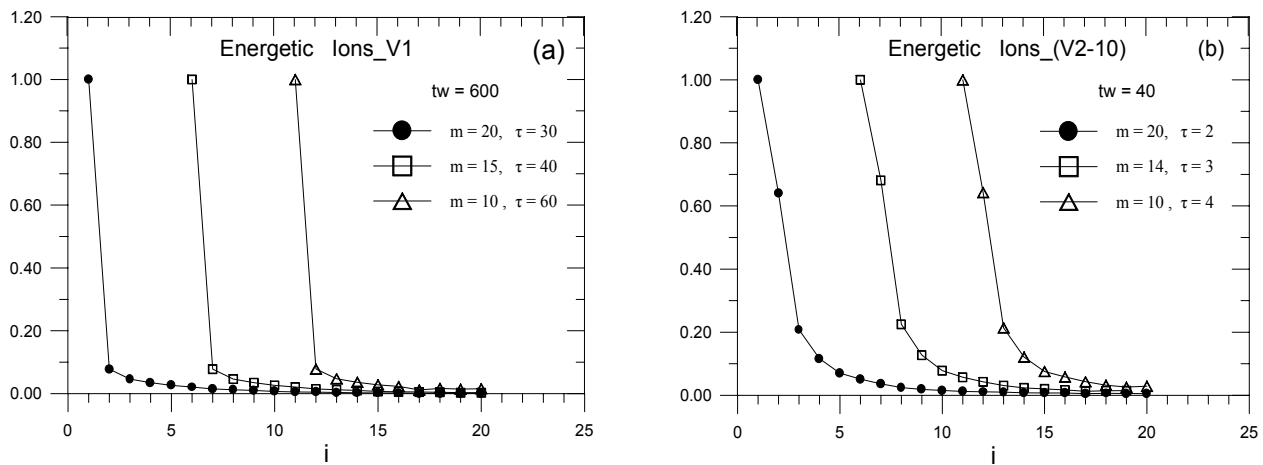


**Fig. 14.** (a, b) The spectra of singular values $\sigma_i$, with parameter $m = 10, 15, 20$, estimated for the SVD reconstructed components $V_1$, $V_{2-10}$ of the magnetospheric energetic ions time series.

autocorrelation coefficient of the $V_1$ component indicates a slow decay profile, while the autocorrelation coefficient of the $V_{2-10}$ SVD component shows a fast decay profile. These characteristics could be explained by a linear stochastic process related to the $V_1$ component and a nonlinear chaotic process underlying the $V_{2-10}$ SVD component in accordance with the results discussed in Sect. 2.5.

The above hypothesis is also supported by the results shown in Fig. 13. Figure 13a presents the slopes of the correlation integrals estimated for the $V_1$ SVD reconstructed component of the energetic ions' time series. This figure reveals that the $V_1$ component does not include any low dimensional characteristic, as there is no satisfactory scaling and low value saturation profile of the slopes. Figure 13c presents the slopes of the correlation integrals estimated for the surrogate data of the $V_1$ component for the embedding dimension $m = 6$. This figure shows that there is no significant difference between the original signal $V_1$ and the surrogate data. As the surrogate data are produced by a nonlinear distortion of a linear noise, we can conclude the linear character of the $V_1$ signal, while the high dimensionality of the $V_1$ component was concluded from Fig. 13a. Based on these results we can support the concept that the $V_1$ SVD component of the ions' time series is basically the manifestation of an external high dimensional coloured noise. This concept is also supported strongly by the similarity which can be observed between the slopes of the ions' $V_1$ SVD component and the $V_1$ SVD component of the Lorenz system perturbed by an external additive coloured noise (see Sect. 2.5).

On the contrary, the $V_{2-10}$ SVD component of the ions clearly reveals low dimensionality and nonlinear characteristics. Figure 13b and d, are similar to Fig. 13a and c including the slopes of the $V_{2-10}$ component and its surrogate data. The scaling and low dimensional profile of the slopes of the $V_{2-10}$ component are clearly indicated by Fig. 13b. The nonlinearly of the $V_{2-10}$ signal is supported by Fig. 13d, as its surrogate data are clearly discriminated by the original signal $V_{2-10}$. The behaviour of the ions' $V_{2-10}$ SVD component corresponds to the behavior of the $V_{2-10}$ component of the coloured noise stochastic Lorenz system (see Fig. 2h). This further strengthens the supposition about the existence of an external high dimensional coloured noise component in the magnetospheric dynamical process underlying the energetic ions' system.

As we have shown in Sect. 2.5, the singular value spectrum of the $V_{2-10}$ component of the Lorenz coloured noise stochastic system is similar to the singular value spectrum of the original purely deterministic Lorenz system. In opposite contrast, the singular value spectrum of the $V_1$ component of the Lorenz coloured noise stochastic system is similar to the spectrum of the original Lorenz stochastic system, i.e. the $V_1$ component absorbs the main part of the external coloured noise perturbation, while the SVD component $V_{2-10}$ remains almost unperturbed by the external coloured noise component, conserving invariant the characteristics of the original (unperturbed) purely deterministic system. The above characteristics of coloured noise stochasticity related to low di-

mensional chaos can be used for understanding the singular spectra of the $V_1$, $V_{2-10}$ SVD components of the energetic ions signal, shown in Fig. 14a–b. Figure 14a presents the singular value spectrum of the $V_1$ component of the ions' time series and Fig. 14b presents the same spectrum for the $V_{2-10}$ SVD component of the ions signal. The singular spectrum of the $V_1$ SVD component of the ions' signal is similar to the singular spectrum of the original time series shown in Fig. 11a, i.e. there is strong asymmetry between the first and the other singular values $\sigma_i$, $i \geq 2$ which are pressed to the noise floor. Contrary to this, the spectrum of the $V_{2-10}$ component is normal, revealing 4–6 nontrivial singular values above the noise background. This analysis can be used to support the central concept described previously, i.e. the $V_1$ SVD component of the ions' time series includes mainly the external coloured noise component, while the $V_{2-10}$ SVD component includes the internal dynamics of the underlying magnetospheric process.

## 4 Summary and discussion

In this work we have estimated the correlation dimension, the false neighbours and the singular value spectrum for the magnetospheric energetic ions measured at the distant magnetotail. In addition, the null hypothesis is tested in order to exclude the case where the original time series arises from a linear stochastic process, but the observed time series may be a nonlinear distortion of the underlying linear time series (Theiler et al., 1992a, b). For the application of the test of the null hypothesis we have used surrogate data constructed according to Schreiber's algorithm, to mimic the amplitude distribution and the power spectrum of the magnetospheric signal. The significance of the discriminating statistics was found to be higher than two sigmas, permitting us to reject the null hypothesis with a confidence greater than 95%.

The correlation dimension was found to be $\sim 3 - 4$, while the false neighbours and the singular value spectrum have shown $\sim 6 - 7$ independent dynamical degrees of freedom. This result is in accordance with the value of the correlation dimension ($D_2$), as the correlation dimension and the maximum number ($n$) of the degrees of freedom are connected by the relation $n \leq 2D_2 + 1$.

Moreover, the SVD analysis has revealed two different physical processes related to the magnetospheric dynamics concluded by the observed energetic ions' signal. The first process corresponds to a stochastic external component, as was indicated by the first SVD component. In this case the test of the null hypothesis has shown that there is no significant difference between the surrogate data and the first SVD component. The second process corresponds to a low dimensional chaotic component, as was indicated by the reconstructed time series obtained by adding the next SVD components. In this case the test of the null hypothesis has shown a strong difference in the discrimination of the surrogate data and the reconstructed time series. In addition, the Lorenz system perturbed by external coloured noise has

shown a strong similarity with the the ion time series according to the above chaotic analysis. In particular, the behaviour of the SVD components of the stochastic Lorenz signal and the magnetospheric ions signal were found to be quite similar for the first component and the reconstructed signal. The comparison of Lorenz's results to those of the ions' signal supports the above concept of two independent underlying physical processes underlying the observed ions signal. The first process may be related to the stochastic dynamics of the solar wind system and the second one to the internal low-dimensional chaotic dynamics of the magnetospheric system. Finally, the above results are in complete agreement with the previous results obtained by the chaotic analysis of magnetospheric $AE$ index.

# References

Abarbanel, H. D., Brown, R., Sidorowich, J. J., and Tsirming, L. S.: The analysis of observed chaotic data in physical systems, Rev. Mod. Phys. 65, 1331–1392, 1993.

Albano, A. M., Muench, J., Schwarzt, C., Mees, A. I., and Rapp, P. E.: Singular value decomposition and the Grassberger Procaccia algorithm, Physical Review A, 38(6), 3017–3026, 1988.

Anagnostopoulos, G. C., Sarris, E. T., and Krimigis, S. M.: Magnetospheric origin of energetic ($E \geq 50$ keV) ions upstream of the bow shock: The October 31, 1977 event, J. Geophys. Res. 91, 3020–3028, 1986.

Anagnostopoulos, G. C., Rigas, A. G., Sarris, E. T., and Krimigis, S. M.: Characteristics of upstream energetic ($E \geq 50$ keV) ion events during intense geomagnetic activity, J. Geophys. Res., 103, 9521–9533, 1998.

Argyris, J., Andreadis, I., Pavlos, G., and Athanasiou, M.: The influence of noise on the correlation dimension of chaotic attractors, Chaos, Solitons, and Fractals, 9, 343–361, 1998a.

Argyris, J., Andreadis, I., Pavlos, G., and Athanasiou, M.: On the influence of noise on the Largest Lyapunov exponent and on the geometric structure of attractors, Chaos, Solitons & Fractals, 9, 947–958, 1998b.

Athanasiu, M. A. and Pavlos, G. P.: SVD analysis of the Magnetospheric $AE$ index time series and comparison with low dimensional chaotic dynamics, Nonlin. Proc. Geophys., 8, 95–125, 2001.

Baker, D. N., Klimas, A. J., McPherron, R. L., and Bucher, J.: The evolution from weak to strong geomagnetic activity: an interpretation in terms of deterministic chaos, Geophys. Res. Lett., 17, 41–44, 1990.

Brogan, W. L.: Modern control theory, Prentice Hall, Englewood Cliffs, New Jersey, 1982.

Broomhead, D. S. and King, G. P.: Extracting qualitive dynamics from experimental data, Physica D, 20, 217–236, 1986.

Broomhead, D. S., Huke, J. P., and Muldoon, M. R.: Linear filters and nonlinear systems, J.R. Statist. Soc. B, 1992.

Casdagli, M., Jardin, D. D., Eubank, S., Farmer, J. D., Gibson, J., Hunter, N., and Theiler, J.: Non linear modeling of chaotic time series: Theory and applications, Los Alamos National Laboratory Preprint LA-UR 91–1637, 1991.

Christon, S. P., Desai, M. I., Eastman, T. E., Gloeckler, G., Kokubun, S., Lui, A. T. Y., McEntire, R. W., Roelof, E. C., and Williams, D. J.: Low-chargestate heavy ions upstream of Earth's bow shock and sunward flux of ionospheric $O^{+1}$, $N^{+1}$, and $O^{+2}$ Ions: Geotail Observations, Geophys. Res. Lett., 27, 2433–2436, 2000.

Ding, M., Grebogi, C., Ott, E., Sauer, T., and York, J. A.: Estimating correlation dimension from a chaotic time series: when does a plateau onset occur?, Physica D 69, 404–424, 1993.

Eastman, T. E. and Christon, S.: Ion composition and transport near the Earth's magnetopause, in: Geophysical monograph 90, Physics of the Magnetopause, edited by Song, P., Sonnerup, B. U. Ö., and Thomsen, M. F., 131–137, 1995.

Elsner, J. B. and Tsonis, A. A.: Singular spectrum analysis, a new tool in time series analysis, Plenum Press, New York, 1996.

Farmer, D. J. and Sidorowich, J. J.: Predicting chaotic time series, Phys. Rev. Lett. 59, 845–848, 1987.

Freeman, T. J. and Parks, G. K.: Fermi acceleration of suprathermal solar wind ions, J. Geophys. Res., 105, 15 715–15 727, 2000.

Goode, B., Cary, J. R., Doxas, I., and Horton, W.: Differentiating between colored random noise and deterministic chaos, J. Geophys. Res., 106, 21, 277, 2001.

Grassberger, P. and Procaccia, I.: Measuring the strangeness of strange attractors, Physica. D, 9, 189–208, 1983.

Ipavich, F. M., Scholer, M., and Gloeckler, G.: Temporal development of composition, spectra, and anisotropies during upstream paryticle events, J. Geophys. Res., 86, 11 153–11 160, 1981.

Kirsch, E., Pavlos, G. P., and Sarris, E. T.: Evidence for particle acceleration processes in the magnetotail, J. Geophys. Res., 89, 1003–1007, 1984.

Klimas, A. J., Baker, D. N., Roberts, D. A., Fairfield, D. H., and Buchner, J. A.: A Nonlinear dynamic model of substorms, Geophys. Monog. Ser., vol. 64, edited by Kan, J. R., Potemra, T. A., Kokumun, S. and Iijima, T., 449–59, AGU, Washington, D.C., 1991.

Klimas, A. J., Baker, D. N., Roberts, D. A., and Fairfield, D. H.: A nonlinear dynamical analogue model of geomagnetic activity, J. Geophys. Res., 97, 12 253–12 266, 1992.

Klimas, A. J., Vassiliadis, D., Baker, D. N., and Roberts, D. A.: The organized nonlinear dynamics of the magnetosphere, J. Geophys. Res., 101, 13 089–13 113, 1996.

Kugiumtzis D.: State space reconstruction parameters in the analysis of chaotic time series-the role of the time window length, Physica D, Vol. 95, 13–28, 1996.

Osborne, A. R. and Provenzale, A.: Finite correlation dimension for stochastic systems with power-low spectra, Physica D, 35, 357–381, 1989.

Pavlos, G. P., Sarris E. T., and Kallabetsos, G.: Monitoring of energy spectra of particle bursts in the plasma sheet and magnetosheath, Planet. Space Sci., 33, 1109–1118, 1985.

Pavlos, G. P.: Magnetospheric dynamics, in: Proc. Symposium on Solar and Space Physics, edited by Dialetis, D., National Observatory of Athens, Athens, 1-43, 1988.

Pavlos, G. P., Rigas, A. G., Dialetis, D., Sarris, E. T., Karakatsanis, L. P., and Tsonis, A. A.: Evidence for chaotic dynamics in outer solar plasma and the earth magnetopause, in: Chaotic Dynamics: Theory and Practice, edited by Bountis, A., Plenum, New York, 327–339, 1992a.

Pavlos, G. P., Kyriakou, G. A., Rigas, A. G., Liatsis, P. I., Trochoutos, P. C., and Tsonis, A. A.: Evidence for strange attractor structures in space plasmas, Ann. Geophysicae, 10, 309–322, 1992b.

Pavlos, G. P., Diamadidis, D., Adamopoulos, A., Rigas, A. G., Daglis, I. A., and Sarris, E. T.: Chaos and magnetospheric dynamics, Nonlin. Proc. Geophys., 1, 124–135, 1994.

Pavlos, G. P., Athanasiu, M., Kugiumtzis, D., Hantzigeorgiu, N., Rigas A. G., and Sarris, E. T.: Nonlinear analysis of Magnetospheric data, Part I. Geometric characteristics of the $AE$ index time series and comparison with nonlinear surrogate data, Nonlin. Proc. Geophys., 6, 51–65, 1999a.

Pavlos, G. P., Kugiumtzis, D., Athanasiu, M., Hantzigeorgiu, N., Diamantidis, D., and Sarris, E. T.: Nonlinear analysis of Magnetospheric data, Part II, Dynamical characteristics of the $AE$ index time series and comparison with nonlinear surrogate data, Nonlin. Proc. Geophys., 6, 79–98, 1999b.

Pavlos, G. P., Athanasiu, M., Diamantidis, D., Rigas, A. G., and Sarris, E.: Comments and new results about the magnetospheric chaos hypothesis, Nonlin. Proc. Geophys., 6, 99–127, 1999c.

Price, C. P. and Prichard, D.: The non-linear responce of the magnetosphere: 30 October 1978, Geophys. Res. Lett., 20, 771–774, 1993.

Price, C. P., Prichard, D., and Bischoff, J. E.: Nonlinear input/output analysis of the auroral electrojet index, J. Geophys. Res., 99, 13 227–13 238, 1994.

Prichard, D. J. and Price, C. P.: Spurious dimensions estimates from time series of geomegnetic indices, Geophys. Res. Lett., 19, 1623–1626, 1992.

Prichard, D. J. and Price, C. P.: Is the $AE$ Index re result of nonlinear dynamics? Geophys. Res. Lett., 20, 2817–2820, 1993.

Prichard, D. J.: Short comment for magnmetospheric chaos, Nonlinear Proc. Geophys., 20 771-20 774, 1995.

Priestley, M. B.: Nonlinear and non-stationary time series analysis, Academic Press, 1988.

Provenzale, A., Osborne, A. R., Kirwan, Jr., A. D., and Bergamasco, L.: The study of fluid parcel trajectories in large-scale ocean flows, in: Nonlinear Topics in Ocean Physics, edited by Osborne, A. R., Elsevier, Paris, 367–402, 1991.

Provenzale, A., Smith, L. A., Vio, R., and Murante, G.: Distinguishing low dimensional dynamics and randomness in measured time series, Physica D, 58, 31–49, 1992.

Roberts, D. A., Baker, D. N., Klimas A. J., and Bargatze, L. F.: Indications of low dimensionality in magnetospheric dynamics, Geophys. Res. Lett., 18, 151–154, 1991.

Sarafopoulos, D. V., Atahanasiu, M. A., Sarris, E. T., Yamamoto, T., and Kokubun, S.: Properties and origin of energetic particles at the duskside of the Earth's magnetosheath throughout a great storm, Ann. Geophysicae, 17, 1121–1133, 1999.

Sarafopoulos, D. V., Atahanasiu, M. A., Sibeck, D. G., McEntire, R. W., Sarris, E. T., and Kokubun, S.: Energetic protons and electrons dispersion signatures in the nightside magnetosheath supporting their leakage out of the magnetopause, J. Geophys. Res., 105, 15 729–15 739, 2000.

Schreiber, T. and Schmitz, A.: Improved surrogate data for nonlin-

earity test, Phys. Rev. Lett., 77, 635–638, 1996.

Schreiber T.: Constrained randomization of time series data, Phys. Rev. Lett., 80, 2105–2108, 1998.

Shan, H., Hansen, P., Goertz, C. K., and Smith, K. A.: Chaotic appearance of the $AE$ Index, Geophys. Res. Lett., 18, 147–150, 1991.

Takens, F.: Detecting strange attractors in turbulence, in: Vol. 898 of Lectures Notes in Mathematics, edited by Rand, D. A. and Young, L. S., 366–381, Springer, Berlin, 1981.

Takens, F.: On the numerical determination of the dimension of an attractor, in dynamical systems and bifurcations, Groningen 1984, in: vol. 1125 of Lecture Notes in Mathematics, edited by Braakama, B. L. J., Broer, H. W., and Takens, F., Berlin, Springer-Verlag, 99–106, 1985.

Theiler, J.: Some comments on the correlations dimensions of $1/f$ a noise, Phys. Lett. A, 155, 480–493, 1991.

Theiler, J., Galdikian, B., Longtin, A., Eubank, S., and Farmer, J. D.: Using surrogate data to detect nonlinearity in time series, in: Nonlinear Modeling and Forecasting, vol. XII of SFI studies in the Sciences of Complexity, edited by Casdagli, M. and Eubank, S., Addison-Wesley, Reading, Mass., 163–188, 1992a.

Theiler, J., Eubank, S., Longtin, A., Galdikian, B., and Farmer, J. D.: Testing for nonlinearity in time series: the method of surrogate data, Physica D, 58, 77–94, 1992b.

Theiler, J., Lisay, P. S., and Rubin, D. M.: Detecting nonlinearity in data with long coherence times, Times series prediction: Forecasting the future and understanding the past, in: SFI studies in the Sciences of Complexity, Proc. Vol. XV, edited by Weigend, A. S. and Gershenfeld, N. A., Addison-Wesley, 429–455, 1993.

Tong, H.: Non-linear time series, a dynamical system approach, Oxford University Press, New York, 1990.

Tsonis, A. A.: Chaos: from theory to applications, Plenum, New York, 1992.

Vassiliadis, D., Sharma, A. S., Eastman, T. E., and Papadopoulos, K.: Low-Dimensional chaos in magnetospheric activity from $AE$ time series, Geophys. Res. Lett., 17, 1841–1844, 1990.

Vassiliadis, D., Sharma, A. S., and Papadopoulos, K.: Time series analysis of magnetospheric activity using nonlinear dynamical methods, in: Chaotic Dynamics: Theory and Practice, edited by Bountis, T., Plenum, New York, 1992.

Vörös, Z.: Synergetic approach to substorm phenomenon, in: Magnetospheric substorms, Geoph. Monog. Ser. Vol. 64, edited by Kan, J. R., Potemra, T. A., Kokubun, S., and Iijima, T., AGU, Washington, D.C., 461–467, 1991.

Weigend, A. S. and Gershenfeld, N. A.: Time Series Prediction: Forecasting the Future and Understanding the Past, Addison-Wesley Publishing Company, Reading, 1994.

Williams, D. J., McEntire, R. W., Schemm II, C., Lui, A. T. Y., Gloeckler, G., Christon, S. P., and Gliem, F.: GEOTAIL energetic particles and ion composition instrument, J. Geomagn. Geoelectr., 46, 39–57, 1994.